Examination of Gilded Bronze using Nondestructive Eddy Current Techniques | 2001-10



National Park Service
U.S. Department of the Interior

National Center for Preservation Technology and Training

Final Report for NCPTT Grant Number MT-2210-9-NC-18

Project title: Examination of Gilded Bronze using Nondestructive Eddy Current Techniques

Applicant organization:
Freer Gallery of Art and Arthur M. Sackler Gallery
Washington DC 20560-0707
202.357.4880 (phone); 202.357.4911 (fax)

Principal investigator:
Blythe McCarthy
Conservation Scientist
Freer Gallery of Art and Arthur M. Sackler Gallery
Smithsonian Institution
Washington DC 20560-0707
202.357.4880 x289 (phone); 202.633.9474 (fax)
mccarbl@asia.si.edu

Project team:
Blythe McCarthy, Conservation Scientist, Freer and Sackler Galleries, Smithsonian Institution, Washington, DC.
Johanna R. Bernstein, Postdoctoral Fellow, Department of Materials Science and Engineering, Johns Hopkins University, 102 Maryland Hall, Baltimore MD 21218
Current address: Corrosion and Protection Centre, UMIST, P.O. Box 88, Manchester, M60 1QD, UK.
James B. Spicer, Associate Professor, Department of Materials Science and Engineering Johns Hopkins University, 102 Maryland Hall, Baltimore, MD 21218.

Table of Contents

Table of Figures ..... **ii**
Table of Tables ..... **iii**
Executive Summary **1**
Introduction **2**
Gilding Types and Characteristics 2
Eddy Currents in Conservation 3
Eddy Current Measurement Techniques 3
Eddy Current Theory 5
Methods and Materials **8**
Methods 8
Reference Samples 9
Results and Discussion **11**
Results – Reference Samples 11
Effect of Composition and Thickness 11
Measurement of Roughness Effects 13
Effect of Subsurface Corrosion or Gilding Delamination 17
Effect of Surface Corrosion, Coating Layer or Lift-off 17
Results - Measurements on Freer Gallery of Art Bronzes 20
Discussion 24
Conclusions **27**
Acknowledgements **28**
References **28**
Appendix A: Analyses of Bronze Disks **30**
Appendix B: Freer Gallery of Art Objects examined using Eddy Currents **30**
Appendix C: Time Domain Measurements **31**

Table of Figures

Figure 1: Induction of eddy currents in a metal, or conductor, by a current carrying coil. 6
Figure 2: Frequency vs critical eddy current depth, t_{cr},. for gold and bronze for four frequency ranges. 7
Figure 3. Cross-sections of (a) leaf gilded sample and (b) mercury amalgam gilded sample. Bar indicates 50 microns..... 10
Figure 4: ?R for Au, Al, Cu, Sn, Pb and bronze sample 10 using (a) 1 – 2.5 MHz, (b) 500 kHz and (c) 50 – 500 kHz probes. The real impedance of air was subtracted from the real part of the impedance for each measurement..... 11
Figure 5: ?R for a series of bronze base metals using (a) 1 – 2.5 MHz, (b) 500 kHz and (c) 50 – 500 kHz probes. The real impedance of air was subtracted from the real part of the impedance for each measurement..... 12
Figure 6: Enlarged view of the curve for (a) Figure 3c and (b) 3d. No difference is seen for this probe between the metals. 13
Figure 7: Frequency vs. ?R for gilded bronze samples with 24K gold layers of varying thickness using (a) 1 – 2.5 MHz, (b) 500 kHz to 1 MHz, (c) 50 – 500 kHz and (d) 5 – 50 kHz. 14
Figure 8: Frequency vs. ?R for gilded bronze samples with gold layers of varying composition, but same thickness, and in composition and thickness for the mercury gilded sample, using (a) 1 – 2.5 MHz, (b) 500 kHz to 1 MHz, (c) 50 – 500 kHz and (d) 5 – 50 kHz.. 15
Figure 9: Frequency vs. ?R was measured for ungilded bronze polished using 250, 400 and 600 grit SiC papers and 6 micron diamond paste using (a) 1 – 2.5 MHz, (b) 500 kHz – 1 MHz, (c) 50 – 500 kHz and (d) 5 – 50 kHz. 16
Figure 10: Frequency vs. ?R for 24K leaf and foil with and without a Mylar interlayer using (a) 1 – 2.5 MHz, (b) 500 kHz – 1 MHz, (c) 50 – 500 kHz) and (d) 5 – 50 kHz. 18
Figure 11. Frequency vs. ?R for samples with different thicknesses of Mylar between sample and probe. Ungilded bronze was examined using (a) 1 – 2.5 MHz and (b) 50 – 500 kHz. Leaf gilded bronze was examined using (c) 1 – 2.5 MHz and (d) 50 – 500 kHz. Foil gilded bronze was examined using (e) 1 – 2.5 MHz and (f) 50 – 500 kHz. 19
Figure 12: Frequency vs. ?R for mercury amalgam gilded bronzes using (a) 1 – 2.5 MHz and (b) 50 – 500 kHz. 21
Figure 13: Frequency vs. ?R for six locations on F1919.81 using a 50 – 500 kHz spot probe. Duplicate measurements on one area are also plotted. All curves represent unaveraged measurements. 21
Figure 14: Frequency vs. ?R for measurement of F1916.445 using 50 – 500 kHz. Data is plotted (a) using two different bronze substrate areas for normalization and (b) as results from both a spot probe and a pencil probe..... 22
Figure 15: Frequency vs. ?R for two samples of unknown gilding for (a) 1—2.5MHz and (b) a 50—500kHz spot probe. Measurements made in triplicate and averaged. 22
Figure 16: Frequency vs. ?R for gilded samples using a 50 – 500 kHz pencil probe. Measurements made in triplicate and averaged at each of three locations for (a) F1913.41a and (b) F1913.42. 23
Figure 17. Frequency vs. ?R for F1980.100, a foil gilded plaque. Each curve is the average of three measurements. 23

Table of Figures, cont.

Figure 18: Frequency vs. ?R for gold, reference sample 15, minus bronze, reference sample 10 for 1-2.5MHz. 25
Figure 19: Frequency vs. ?R with error bars for Hg gilded bronze and 24K leaf gilded bronze for (a) 1 – 2.5 MHz and (b) 5 – 50 kHz. 26
Figure A2.1a-d. Change of voltage with time for gilded samples measure with four different probes. 32

Table of Tables

Table I: Gilding Methods And Their Characteristics 3
Table II: Critical Thickness Ranges 7
Table III. Probe Characteristics 8
Table IV: Characteristics of Reference Samples 9
Table V: Compositions of Materials Used in Reference Samples in Weight Percent 10
Table VI: Roughness Values of Bronze Surface. 16
Table VII: Thickness of Mylar Placed Above Samples. 17

Executive Summary

Eddy current testing methods were used to characterize model gilding layers on bronzes and to make measurements on gilded bronze objects in the Freer Gallery of Art. Swept frequency eddy current measurements were able to discern differences between gilding layers of varying thickness, and also between gilding layers of varying composition, i.e. conductivity, on a series of reference samples. Measurements made on the Freer Gallery objects were consistent with reference sample results for mercury amalgam gilding.

The critical depth of penetration of the eddy currents was calculated for gold and bronze for each of the four frequency ranges used. A simple model was developed to describe the influence of the different types of gilding layers on the change in probe impedance resulting from the interaction of the sample and probe. The model treats gilding layers of three different thickness ranges separately. In the first case, the gilding layer thickness is less than the critical depths for gold or bronze, $t_{\text{Au layer}} < t_{\text{cr(Au)}}$. , $t_{\text{cr(bronze).}}$ In the second case, the gilding layer thickness is greater than the critical depth for gold, yet less than the critical depth of the bronze, $t_{\text{cr(Au)}} < t_{\text{Au layer}} < t_{\text{cr(bronze)}}$, and in the third case, the gilding layer thickness is greater than the critical depth for both gold and bronze, $t_{\text{cr(Au)}}$, $t_{\text{cr(bronze)}} < t_{\text{Au layer}}$.

Variations in the bronze substrate composition and microstructure influence the measurements. Thus a differential measurement was used in this study for the gilded surfaces, normalizing the raw data by a measurement on a bare bronze surface. Surface roughness was found to influence results at high frequencies where the roughness is much less than the eddy current critical depth for the metal. Experiments using nonconducting Mylar were undertaken to model the effect of surface and subsurface corrosion, and lift-off. It was concluded that surface corrosion, and similarly lift-off, will decrease the eddy current penetration depth into the sample. Subsurface corrosion does not affect eddy current penetration into the gilding layer, but does decrease penetration into the bronze substrate. In both cases, the relative effect of the substrate and gilding layer on the probe impedance change due to the presence of the corrosion.

By making measurements at two frequency ranges, one at low frequency and one at high frequency, it was possible to discriminate between samples gilded using several different gilding techniques, including electrochemical methods, leaf gilding, mercury amalgam gilding, and foil gilding.

A second eddy current technique that uses a pulsed excitation source was briefly explored. The technique was able to discriminate between samples with 24K gold leaf, 23.5K gold leaf and 24K foil gilding.

Introduction

Gilding, the application of gold and gold alloys to the surface of baser metals, is found throughout the world. Different techniques have been used to form gilded surface layers of various chemical compositions, thickness and uniformity. Numerous technological studies of gilded objects have been undertaken using chemical and microscopical techniques to gather information about gilding methods across cultures and over time. However, these techniques can be inadequate or inappropriate because only limited sampling of museum objects and archaeological artifacts is possible, if sampling is at all permitted. The use of nondestructive eddy current measurements can overcome these sampling limitations.

Eddy current methods have been used extensively in industry for the examination of metals. (ASNT 1986). The use of the eddy current technique, wherein a probe causes an electrical current in a metal, is used to detect flaws and areas of corrosion, measure the thickness of surface films (conducting and nonconducting) on metal substrates of differing electrical conductivity and distinguish between different alloys, heat treatments or processing methods. This study extends the use of eddy current techniques into the field of conservation, using this method to examine gilding on reference samples and bronze objects.

Gilding Types and Characteristics

A number of studies have identified several types of gilding processes on bronze objects, including fire gilding, gilding with foil or leaf, and electrochemical replacement methods (Lechtman 1979; Oddy 1993; Scott 1983). The different processes result in gilding layers of differing chemical composition, thickness and uniformity. Fusion gilding involves the application of a molten alloy of lower melting temperature to the substrate metal (Bray 1993). Fire gilding involves the application of a gold mercury amalgam to the base metal with subsequent heat treatment to drive off some of the mercury (Jett 1993). Gold foil and gold leaf are sheets of gold or gold alloys which are applied to the base metal and bonded using heat (diffusion bonding), mechanical bonds or an adhesive material (Oddy 1993). Electrochemical replacement and plating techniques both involve deposition of metal from a solution containing metallic ions. (Lechtman 1979). In depletion gilding, the surface of the object, either a solid gold alloy or a metal object with a gold alloy layer at the surface, is enriched in gold by the removal of the alloying elements through etching (Lechtman 1973; Scott 1983). Much of the research to date on gilded bronzes is summarized in the recent volume, *Gilded Metals* (Drayman-Weisser 2000). Some of the differences in layer characteristics of the various gilding methods are summarized in Table I.

It is sometimes possible to discriminate between gilding methods by visual observation; for example, leaf and foil techniques can leave evidence of overlapping pieces of gold, while fire gilding can cause a rough, crystalline surface in crevices and inscribed lines which would not have been burnished. However, these distinctions are not always possible, and require further analysis. Conservation scientists can also examine gilding layers on metals through observation using low power optical microscopes, chemical analysis and metallographic techniques. With the advent of larger chambers in scanning electron microscopes, it is sometimes possible to examine whole objects, such as coins, at higher magnification. This is not, however, possible for larger objects and statuary.

In addition, there are standard industrial methods of analysis. The American Society for Testing and Materials has a standard guide, B659-90, for measuring the thickness of metal and inorganic coatings which lists nondestructive, semi-destructive and destructive methods (ASTM 1998). Nondestructive methods for analysis of non-magnetic materials include a beta-radiation backscatter method, x-ray fluorescence (XRF) methods and an eddy current method. Both the XRF and beta-backscattered

methods were developed to measure the thickness of metallic coatings, but have serious limitations. For example, results from both XRF and beta-backscattered techniques can be influenced by the presence of corrosion products leading to possible misinterpretation of results. In addition, the ASTM eddy current method is designed specifically for measuring the thickness of nonconductive coatings on nonmagnetic substrate metals, and does not address metallic coatings.

Table I: Gilding Methods And Their Characteristics

Gilding method	Layer thickness	Layer Characteristics
Fusion gilding	varies	non-uniform thickness, alloyed gold of lower melting temperature than substrate
Fire gilding	micrometers to tens of micrometers	non-uniform thickness, contains mercury
Gold foil	micrometers to tens of micrometers	uniform over single sheet, areas of overlap
Gold leaf	tenths of micrometers	uniform thickness over single sheet, areas of overlap
Electrochemical replacement	0.5 - 2 micrometers	uniform thickness

Eddy Currents in Conservation

Eddy currents have been used in the field of conservation to identify areas of gilding under a later paint layer (Mundry and Riederer 1988) and to determine the thickness of corrosion layers (Mach, Poehlmann, and Stoeckle 1991). Eddy current techniques were used by Marabelli and Medori in their examination of the "Bronzi di Riace"(Marabelli and Medori 1991). Using a frequency range of 200-300 kHz, they were able to detect the presence of weldings, cracks and repairs in the bronze. Although they were reporting on initial investigations, they felt the technique had potential for monitoring crack growth in sculptures. They were also able to follow variations in conductivity, however the source of the variations was not determined but was given as one of several microstructural or processing parameters. Defects were also identified in the iron clock tower of F. Borromini in Rome by Bartolini et. al. using similar magnetoscopic techniques (Bartolini et al. 1997).

No examples of the use of eddy current techniques to measure thickness or conductivity of coating layers were found in the conservation literature.

Eddy Current Measurement Techniques

Eddy current techniques are used in several industries as a nondestructive plant inspection tool and for process management. For example, in the power industry, eddy current methods used to measure the integrity of tubular heat exchangers by detecting any cracks or flaws present at or near the surface. Other examples of industrial applications include for the auto industry, the measurement of the thickness of tin applied to steel pistons that provide lubrication, and for aerospace applications, the detection of corrosion in the skin of aluminum fuselages(ASNT 1986).

Eddy currents can also be used to characterize microstructure. Mel'nikov et. al. used a probe with ferrite core to measure changes in the surface of steel specimens due to varying grinding and finishing regimens. They could correlate the surface with the eddy current signal (Mel'nikov et al. 1998). In eddy current studies of zinc coated aluminum alloy parts, Brainin et. al. found that the standards used to calibrate the thickness meters they were using needed to undergo the same pretreatments prior to metallization as the samples under study(Brainin et al. 1993). Current research in measurements of

microscale properties of materials through use of scanning probe microscopy have utilized eddy currents. High resolution (100 micron) mapping of defects in copper film was performed using a scanning magnetic probe (Palmer, Drew, and Decca 2000).

Eddy currents have also been used to measure the thickness of non-conducting surface layers on metals, and a number of commercial thickness gauges based on eddy currents are available for the measurement of nonconducting coatings. They require calibration on a metal of similar metallurgical composition to that being tested in the range of coating thicknesses of interest. The use of commercial thickness gauges for determining the thickness of conductive coatings may give rise to significant errors and is not recommended (Cunningham 1995). However, there is significant interest in characterizing conductive surface layers. Researchers have been active in this area more recently, and there are several pertinent eddy current studies of multilayer conductive materials. In early work, Dodd and Deeds developed analytical solutions that modeled the interaction of a coil with a metallic plate clad with a layer of different conductivity. Their models, which agreed well with experimental results, have formed the basis for most of the studies of thickness and conductivity of coatings on metallic substrates (Dodd and Deeds 1968).

Sandovskii calculated the sensitivity of eddy current transducers to changes in coating thickness and electrical conductivity at selected single frequencies. He compared the sensitivity of changes in amplitude to the sensitivity of changes in phase of the eddy current signal caused by the presence of a conducting coating on a metallic substrate. His calculations showed that using phase analysis is more sensitive to changes in thickness and by using the correct experimental conditions one can negate the effect of changes in conductivity of the coating (Sandovskii 1994).

Norton et. al. used multi-frequency eddy current measurements to determine conductivity profiles in two cases with cylindrical symmetry: a case with two layers of discrete conductivities and the case of a smoothly varying conductivity profile (Norton, Kahn, and Mester 1989). They used an inversion method to determine values of conductivity and the position of the interface between the two layer from impedances measured at 23 frequencies.

Uzal et al. modeled and experimentally determined the changes in impedance due to the presence of surface layers whose conductivity varies as a function of depth. Their model looked at a sample with a conductivity profile in the shape of a hyperbolic tangent. Experimentally they studied samples formed of thin films of varying conductivity arranged atop one another to mimic various conductivity profiles, and also examples of case-hardened titanium which provided a true example of a diffusional profile. They found that the differences in the impedance due to the surface layer are largest when the difference in conductivity is localized at the surface. They found that the imaginary part of the impedance dominates the change in voltage detected by the probe (Uzal et al. 1993).

Moulder, Uzal and Rose were able to determine both thickness and conductivity independantly if the thickness was between 0.2 to 0.5 times the coil radius. For the coils they used the minimum thickness for such a measurement was approximately 100 microns. For thinner surface layers, they found that the impedance was proportional to the product of the thickness and the difference in conductivity between the surface layer and the substrate. In these cases they were only able to calculate one of the two parameters, thickness or conductivity if the other was already known. They suggested that smaller diameter probes with ferrite cores, thus producing stronger signals, might be more useful for measurement of thinner surface layers. Their data analysis concentrated on the real portion of the impedance, or resistance, finding that the uncertainties due to coil geometry were more serious in the reactance. In addition, the resistance exhibited more features in the frequency domain than the reactance, allowing for feature based data analysis. The resistance has a minimum or maximum and a zero crossing, whereas the reactance is a first order curve. To obtain accurate results, they found that

they needed to use data including a zero crossing and continuing up to twice the frequency where the zero crossing was found (Moulder, Uzal, and Rose 1992).

To correct for deviations from theory of the data caused by capacitance of the coil which at high frequency leads to resonance of the measurement circuit, Tai, in his similar studies of swept frequency measurements on magnetic metals, used corrections developed by other researchers, (Harrison, Jones, and Burke 1996). He calculated a parallel impedance that increased with increasing frequency, representing the deviation of the coil impedance from the ideal zero capacitance value. This was subtracted from the measured impedance. Such a correction could also be used in measurements of nonmagnetic metals(Tai 2000).

A faster method of data analysis for frequency domain analysis was introduced where the data was rescaled using three parameters derived from curves of the difference in resistance versus frequency: w, the height at the maximum or minimum of the curve, f_w, the frequency where the maximum occurs, and f_o, the frequency where the zero crossing occurs(Sethuraman and Rose 1995). This significantly reduced the time necessary to calculate the conductivity and thickness of the surface layer relative to that required in an earlier method (Moulder, Uzal, and Rose 1992) which used 20 points from the curve of the difference in resistance versus frequency. Additionally the same researchers corrected the data for what they believed was thermal drift by raising or lowering the curves so that they initiated at the origin. This does not, however, overcome the problems associated with independant determination of conductivity and thickness detailed by Moulder et. al. In their experiments, they looked at measurements of stepped thicknesses with the coil placed on each step and halfway between each step. They were able to determine a good value for each of the steps. In the case where the coil was inbetween the two steps, they obtained a value of thickness inbetween that of the two layers.

Measurements of the thickness of conductive nonmagnetic coatings on ferromagnetic substrates have also been made for the case of cylindrical symmetry (de Halleux, Ptchelintsev, and Stirum 1997). The method worked best for coatings of thicknesses greater than 12microns. For coatings less than 12 microns thick it was necessary for them to introduce an apparent conductivity and a thickness offset into their calculations to obtain agreement between theory and experiment.

Eddy Current Theory

Eddy current measurement techniques are based on the creation of eddy currents in an electrically conductive material. To produce the eddy currents, a probe, essentially a coil, is excited by an alternating current, creating a time varying magnetic field. The magnetic field induces eddy currents in a nearby electrically conductive material, or sample, as shown in Figure 1. The

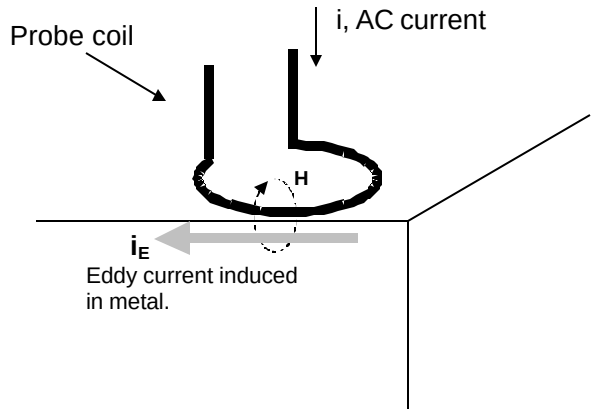


Figure 1: Induction of eddy currents in a metal, or conductor, by a current carrying coil.

currents create a secondary opposing magnetic field, which interacts with the magnetic field of the probe. This interaction is monitored by measuring any changes in the probe's electrical impedance. Factors affecting the flow of eddy currents within the material, i.e. changes in electrical conductivity and magnetic permeability, will be reflected as changes in the probe's impedance, although for low-iron bronze and gold, the magnetic permeability has virtually no effect. These changes can also be related to the physical properties of the sample such as thickness of a surface film.The operating frequency, probe size, and the distance between the probe and the test object, known as "lift-off", will determine the sensitivity of detection.

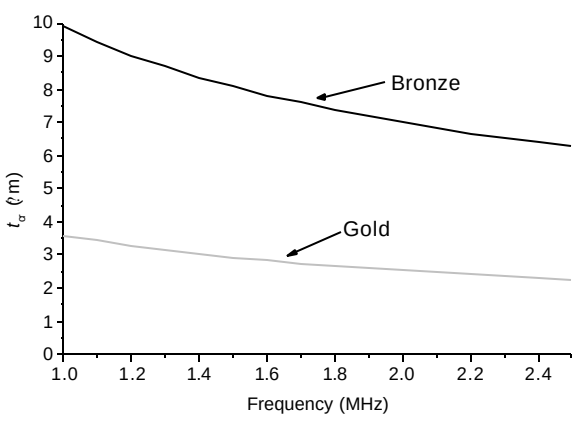
Eddy current techniques are essentially surface techniques, their magnitude decreasing exponentially with depth.. The effectiveness of the technique is based on the interaction of the surface of the probe and the surface of a conducting material. A key parameter is the standard depth of signal penetration, or skin depth, that is a function of the conductivity and magnetic permeability of the material, and the operating frequency of the probe. As the operating frequency increases, the depth of penetration decreases. The skin depth is the distance from the surface to the layer in which the eddy currents are equal to 0.37 of their initial value, which may be calculated using

$$? \; ? \; \frac{1}{\sqrt{? \; ? \; ? f}} \qquad (1)$$

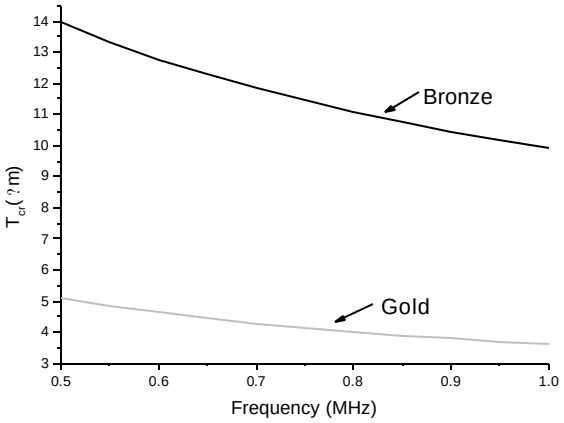
where ? is the magnetic permeability, equal to 1 for non-ferromagnetic materials such as bronze and gold, ? is the conductivity and ?is the probe frequency. However, the eddy currents still penetrate beyond this depth and can affect measurements. Thus, it is necessary to consider the depth at which attenuation becomes large enough that the electromagnetic field can be neglected (Silkin and Ponomarev 1994). This critical depth, t_{cr}, is related to the skin depth by

$$t_{cr} = (? / 2)? \; = 1.57? \qquad (2)$$

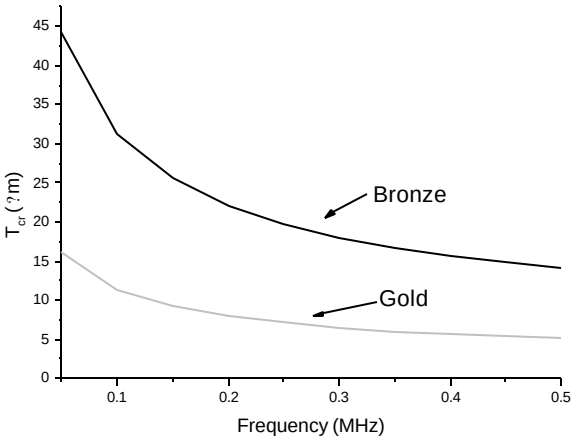
The critical depth was calculated for gold and bronze for each of the four frequency ranges used in this study. The results of the calculations are plotted in Figure 2 and given in Table II. The critical depth calculations as presented, are approximations, they do not account for the presence of the ferrite core in the probes used in this study. The ferrite core acts on the magnetic fields, effectively focusing them and increasing the critical depth.



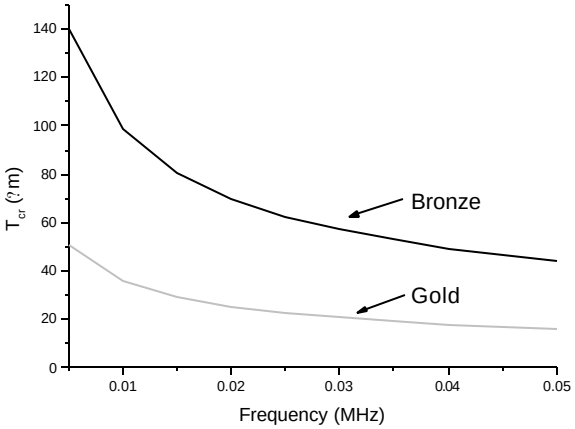
(a)



(b)



(c)



(d)

Figure 2: Frequency vs critical eddy current depth, t_{cr},. for gold and bronze for four frequency ranges.

Table II: Critical Thickness Ranges

	5 – 50 kHz (mm)	50 – 500 kHz (mm)	500 – 1000 kHz (mm)	1 – 2.5 MHz (mm)
Au	0.016 – 0.036	0.0050 – 0.0160	0.0036 – 0.0050	0.0022 – 0.0036
Bronze	0.044 – 0.140	0.0140 – 0.0443	0.0099 – 0.0140	0.0063 – 0.0099

For coated materials in which the eddy current penetration depth is larger than the coating thickness, as coating thickness increases or decreases, the measured impedance will depend on changes in the composite properties of the coating and the substrate. The change in impedance may be used to measure the coating thickness when the critical depth of eddy current penetration is greater than the coating thickness. For a high conductivity coating on a lower conductivity material, the impedance measured with increasing coating thickness proceeds nonlinearly from the value that would be measured from the substrate material alone, to that of the coating (ASNT 1986). Plots of the real (resistance) versus the imaginary (reactance) components of the impedance produce a clockwise spiral, or conductivity locus, which can be correlated to coating thickness. Changes in the conductivity locus can be correlated to the presence of a layer of a nonconductive material, such as a corrosion product (Hagemaier 1990).

Methods and Materials

This study was conducted in two parts. In the first part, reference samples made of model materials were examined. In the second part, gilded bronzes from the collection of the Freer Gallery of Art were examined. Of the Freer bronzes, two groups were examined: those whose surfaces had already been well characterized in a previous study, and those whose surface gilding technique had not yet been determined.

Methods

Eddy current spot probes (Zetec Catalogue Nos. 910-4801, 4802, 4803 and 4804) were used to characterise the prepared gilded bronze samples. Five replicate measurements, each the average of 16 scans were made on each sample. The active diameters and frequency ranges of the probes are given in Table III. Changes in probe impedance were measured with an impedance analyser (Hewlett Packard HP4194A) in sweep mode corresponding to the frequency bandwidth of the probe. All measurements of gilded samples were normalized by a reference measurement from an ungilded bronze sample. Previous research has shown that the real portion of the impedance contains fewer uncertainties than the imaginary component(Moulder, Uzal, and Rose 1992), thus, this study concentrated on measuring changes in the real part of the impedance, or resistance, R. Raw resistance signals were normalized by subtracting the resistance measured for an ungilded bronze sample from the raw resistance of the gilded samples. For measurements of ungilded metal samples, an open circuit measurement was subtracted from the resistance of the samples. Plots were then made of ?R vs. frequency to determine the most effective operating frequency ranges for characterizing gilding layers.

Table III. Probe Characteristics

Probe Number	Frequency Range	Active Diameter
910-4801	5—50kHz	.375"
910-4802	50—500kHz	.125"
910-4803	500kHz—1MHz	.125"
910-4804	1Mhz—2.5MHz	.100"
909-0030	50—500kHz	Pencil probe

Reference Samples

Reference samples were made by gilding 4 cm^2 bronze pieces prepared with 600 grit SiC to form models of the gilding types listed in Table I. The bronze material chosen for the substrate was cut from an ingot cast by Colonial Metals Co. (Alloy #305). The bulk composition for the ingot in weight percent was Cu 79.21, Sn 9.46, Pb 9.95, Fe 0.06, Sb 0.38, Ni 0.30, and Zn 0.60.

Fourteen gilded bronze reference samples were made using electroless plating, three compositions of gold leaf, gold foil, and mercury amalgam gilding. Gilding methods for each sample are listed in Table IV. Sizing was used to attach the leaf and foil layers. Modifications to the method are noted in the table. To explore the effect of lack of contact between the gilding layer and the bronze substrate, such as might be found in a corroded bronze, a thin sheet of Mylar was introduced between the gilding layer and the bronze on three of the samples. In addition, a piece of pure gold, and a sheet of Mylar were also examined. Finally, measurements were made of a series of bronze disks, commissioned by R. J. Gettens in 1963, to represent a variety of bronze compositions, to examine the effect of varying substrate composition. Wet chemical analyses of the bronze disks are given in Appendix A.

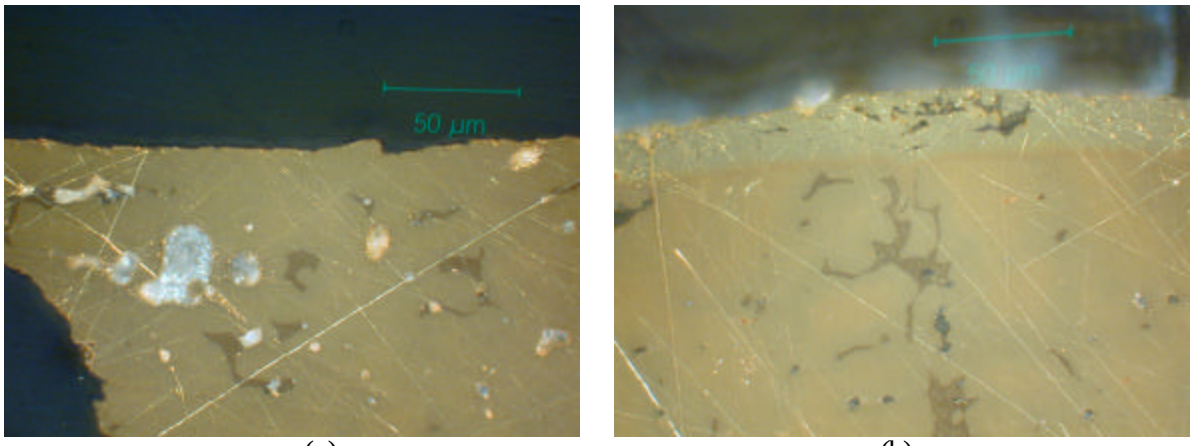
Table IV: Characteristics of Reference Samples

Sample	Gilding method	nominal gold composition	Avg.(5) thickness microns	Std. Dev.	Comments
1	Electroless gold	Au 100%	0.07	0.01	None
2	24K leaf	Au 100%	0.1	0.01	None
3	Edible gold leaf (23K)	Au 97%Ag3%	0.14	0.01	None
4	Hg-Au amalgam	---	28.42	17.2	Approx. 6:1 Hg:Au, then heated to remove Hg
5	Red gold leaf (23.5K)	Au 97.5%Cu 2.5%	0.12	0.01	None
6	24K foil	99.95% pure Au	50	----------	Mylar under gold
7	24K foil	99.95% pure Au	50	----------	None
8	24K Leaf	Au 100%	.1	.01	Mylar under gold
9	Not used				
10	Bare bronze	----------	----------	----------	No gilding
11	24K leaf – 2 layers	Au 100%	.2		
12	24K leaf – 4 layers	Au 100%	----------	---------	----------
13	24K leaf – 4 layers	Au 100%	----------	---------	No size used
14	24K foil	99.95% pure Au	50	---------	Mylar under gold attached to substrate only at corners
15	24K foil only	99.95% pure Au	50	---------	No substrate
16	Mylar only	----------	3.81	---------	No substrate

Before eddy current testing, the microstructure and composition of the samples were characterized. The microstructure of the leaf gilded bronze substrate, shown in Figure 3, was examined in cross-section and compared to that of the mercury amalgam gilded bronze reference sample that was heated during the gilding process. No significant difference was observed. The microstructure of the bronze consists mainly of alpha phase exhibiting coring, with small areas of delta phase and segregated lead-rich areas. Average porosity measured 5%.

The thickness of the gilding layers was measured using scanning electron microscopy. Composition of the gilding layers was determined using x-ray microanalysis. To obtain quantitative measurements without interference from the bronze substrate, it was necessary to mount samples from the gold leaf separately for this analysis because of the thinness of the gold layer. Samples were taken from the same sheets as those used to gild the reference samples. Compositional analysis is summarized in Table V.

In addition to material characterization, the surface roughness as a function of degree of polish was measured using a Taylor Hobson Surtronic 3+ profilometer.. The same bronze (alloy #305) as used for the reference samples was prepared using wet SiC grinding paper, and roughness measurements were made after finishing to grit sizes of 250 and 600. Measurements were also made after polishing using a 6 micron diamond suspension



(a) (b)

Figure 3. Cross-sections of (a) leaf gilded sample and (b) mercury amalgam gilded sample. Bar indicates 50 microns.

Table V: Compositions of Materials Used in Reference Samples in Weight Percent

Gilding Type	**Au**	**Hg**	**Ag**	**Cu**	**Sn**
electroless*	90.63	--	--	7.96	1.4
24K leaf	100.00	--	--	--	--
23K leaf	95.31	--	4.69	--	--
Hg amalgam gilding	77.86	21.83	--	--	--
23.5K	97.47	2.53	--	--	--

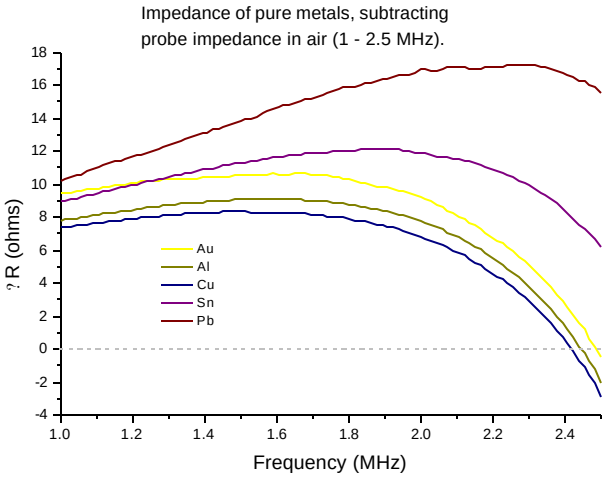
* The electroless plated layer was too thin to obtain a valid composition and the copper and tin are included from interference from the underlying bronze.

Results and Discussion

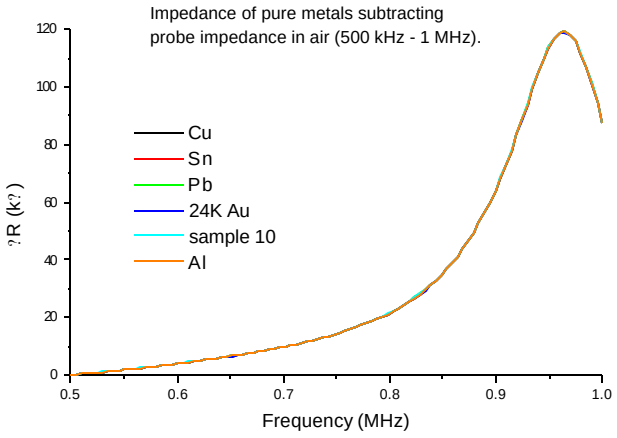
Results – Reference Samples

Effect of Composition and Thickness

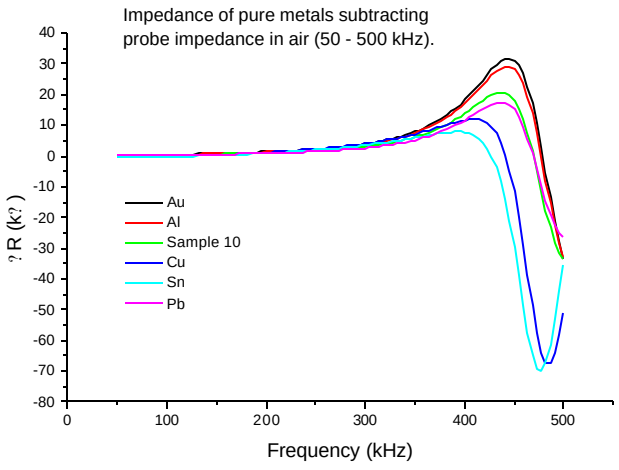
Measurements were made on a series of base metals, Figure 4, and of a series of bronze disks, Figure 5. The gold sample, whose data is shown in Figure 4, is listed as sample 15 in Table IV. There is variation in the real impedance measured for the different samples in all cases but that of the 500kHz to 1MHz probe. The difference for these curves are negligible, even on closer inspection, as shown in Figure 6. This is likely to be a result of a wiring problem with the probe when the measurements were taken. The problem was subsequently fixed. Also note that the impedance characteristics for each probe are sufficiently different so that the data cannot be merged to give a full range from 5 kHz to 2.5 MHz and must be analyzed separately for each probe range.



(a)

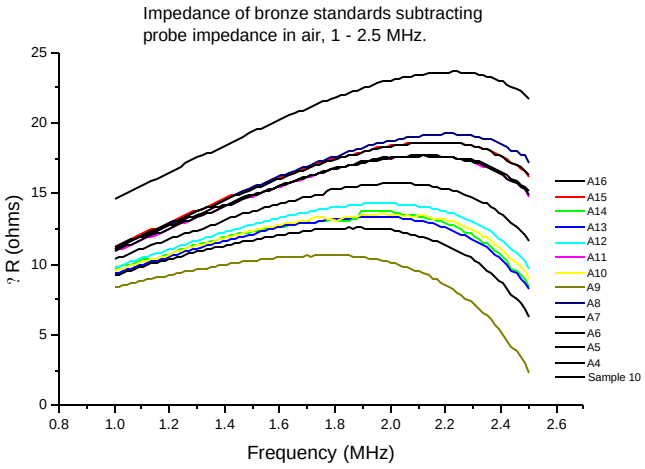


(b)

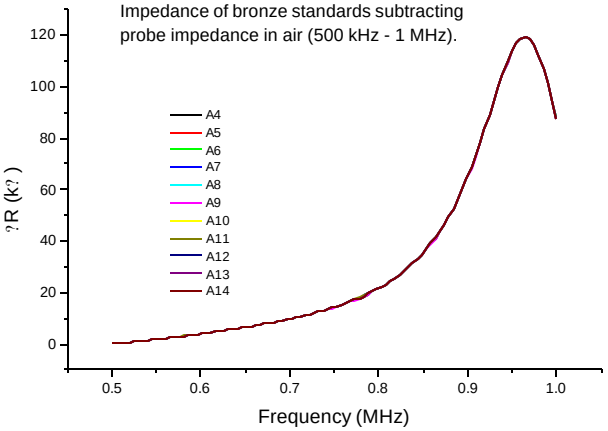


(c)

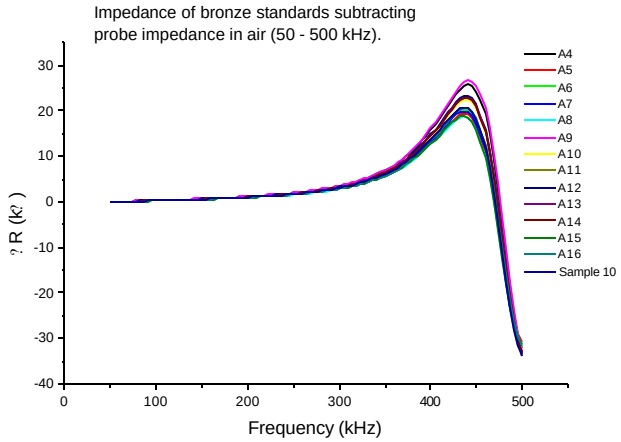
Figure 4: ? R for Au, Al, Cu, Sn, Pb and bronze sample 10 using (a) 1 – 2.5 MHz, (b) 500 kHz and (c) 50 – 500 kHz probes. The real impedance of air was subtracted from the real part of the impedance for each measurement.



(a)

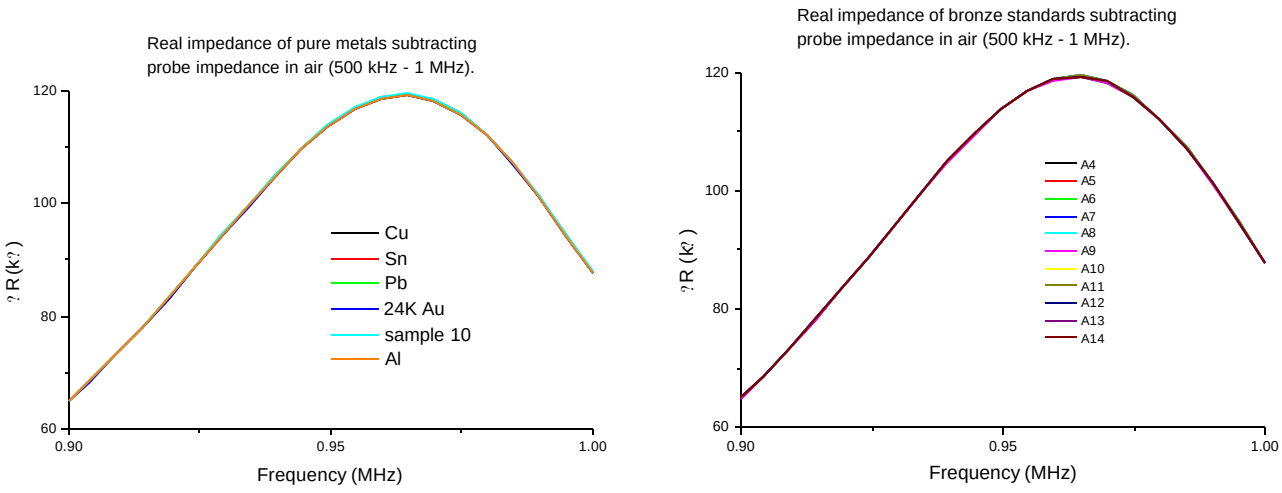


(b)



(c)

Figure 5: ? R for a series of bronze base metals using (a) 1 – 2.5 MHz, (b) 500 kHz and (c) 50 – 500 kHz probes. The real impedance of air was subtracted from the real part of the impedance for each measurement.



(a) (b)

Figure 6: Enlarged view of the curve for (a) Figure 3c and (b) 3d. No difference is seen for this probe between the metals.

Data subsets taken with each of the four probes are shown in Figures 7 and 8, organized according to samples with varying gilding layer thickness, Figure 7, and with varying composition, Figure 8. In Figure 8, the curves for the Hg gilded sample are included even though the Hg gilded layer is thicker than the leaf layers. This serves to show the influence of skin depth effects. Figures 8(c) and (d) show the effect clearly. The signals from the Hg gilded sample completely change polarity or slope from the others. In Figures 8(a) and (b), the differences are less clear. For the results from the highest frequency probe, shown in Figure 8(a), the eddy current skin depth does not penetrate into the bronze substrate so that the probe is only measuring differences in composition, and possibly microstructure of the gold. For the results from the next highest frequency probe, shown in Figure 8(b), the effect is less dramatic, although it appears that the curve for the Hg gilded sample has changed the sign its slope compared to the other curves. This suggests that the thickness of the gold layer is affecting the signal since the eddy current skin depth is now penetrating the bronze substrate, although not as far as for the two lower frequency probes.

Measurement of Roughness Effects

The results of measurements made on bronze substrates of varying degrees of surface roughness are plotted in Figure 9. The arithmetic mean of the departures of the surface profile from the mean line of the profile (R_a) are reported in Table VI. There is little difference in signal due to roughness effects except for the highest frequency range, 1 – 2.5 MHz. If the actual roughness is small compared to the skin depth, the effect of roughness will be small. This is the case for the lower frequency range probes. However, if the actual roughness is on the order of the skin depth, such as for the higher frequency probes, there will be a noticable effect.

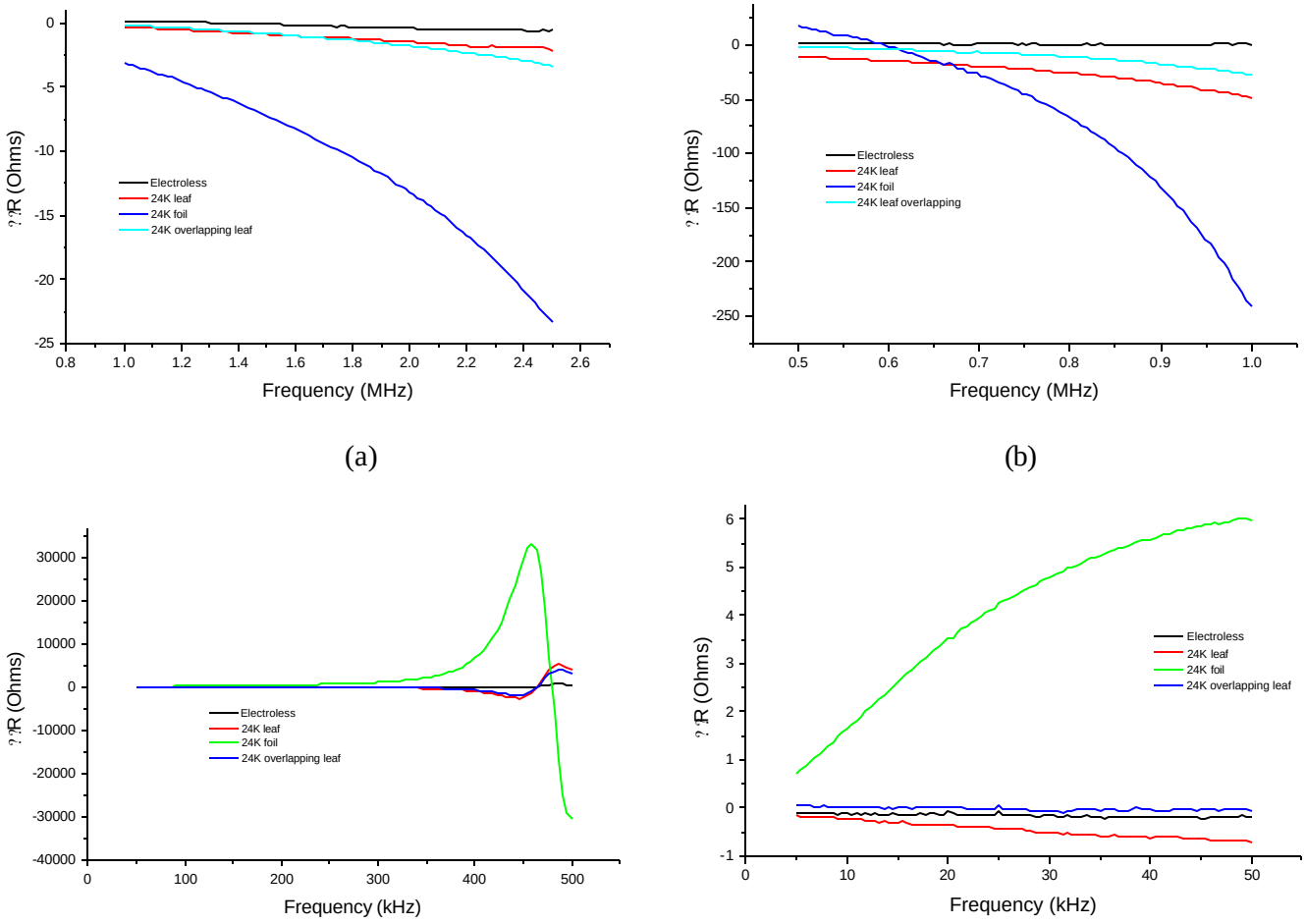


Figure 7: Frequency vs. ?R for gilded bronze samples with 24K gold layers of varying thickness using (a) 1 – 2.5 MHz, (b) 500 kHz to 1 MHz, (c) 50 – 500 kHz and (d) 5 – 50 kHz.

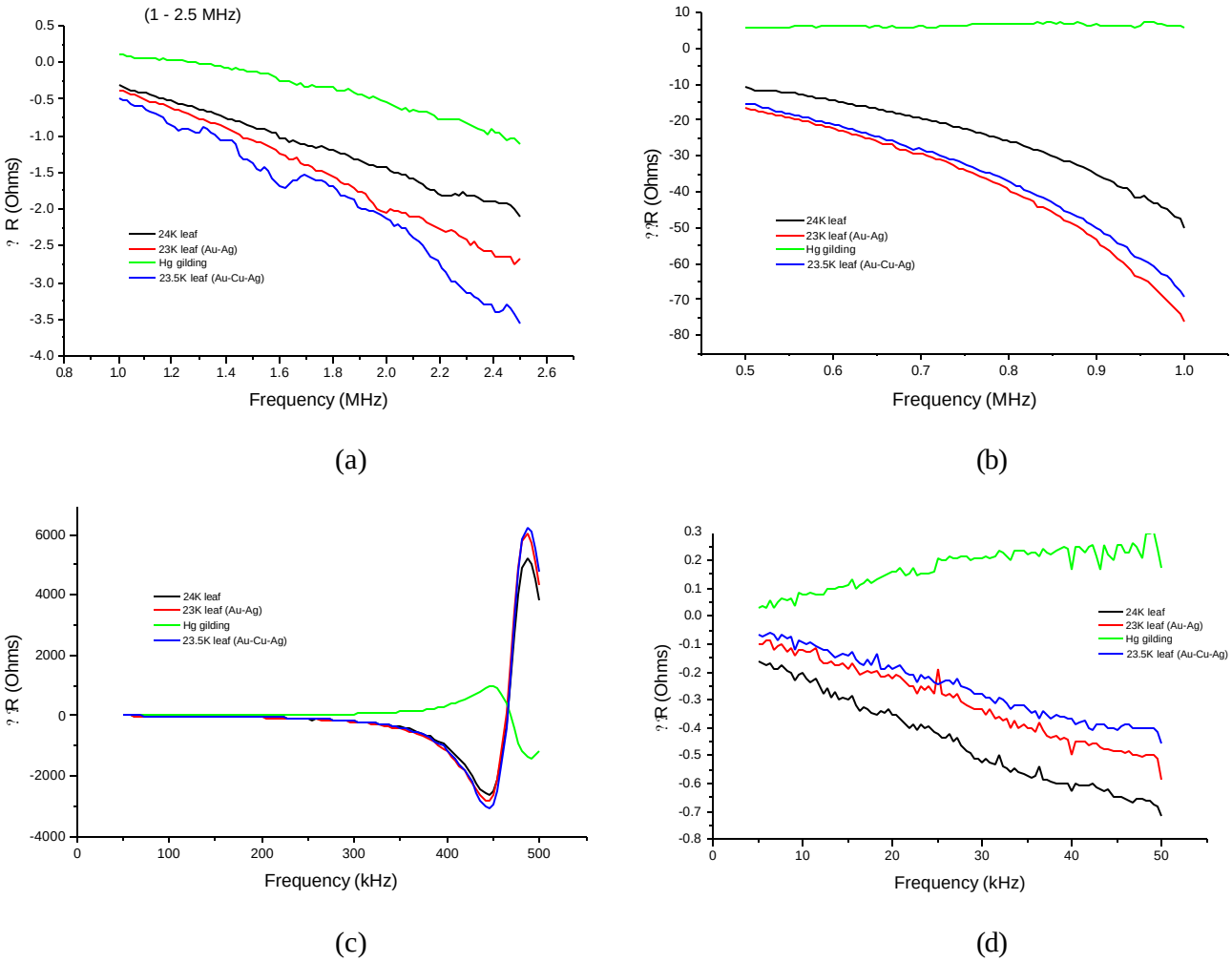


Figure 8: Frequency vs. ? R for gilded bronze samples with gold layers of varying composition, but same thickness, and in composition and thickness for the mercury gilded sample, using (a) 1 – 2.5 MHz, (b) 500 kHz to 1 MHz, (c) 50 – 500 kHz and (d) 5 – 50 kHz

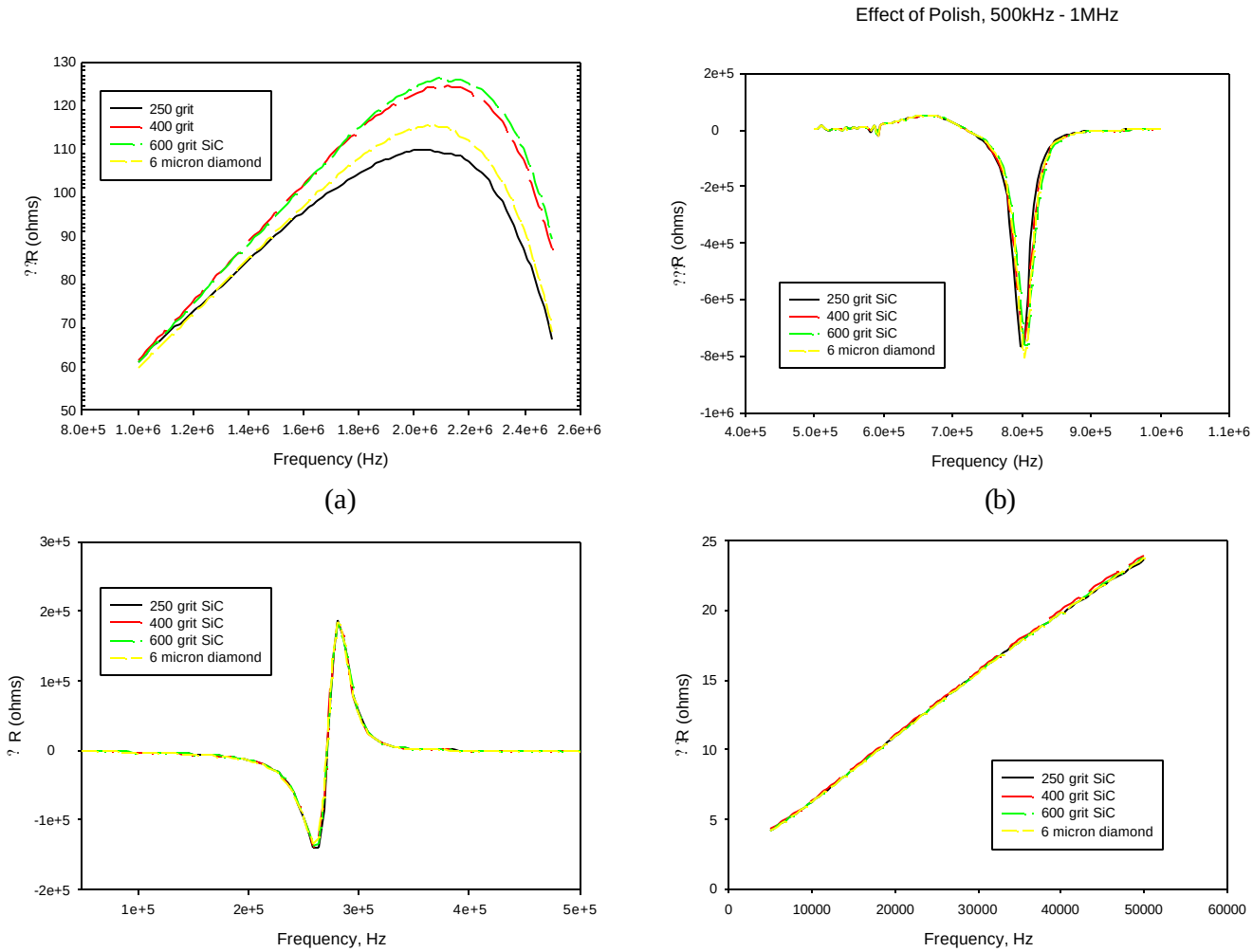


Figure 9: Frequency vs. ? R was measured for ungilded bronze polished using 250, 400 and 600 grit SiC papers and 6 micron diamond paste using (a) 1 – 2.5 MHz, (b) 500 kHz – 1 MHz, (c) 50 – 500 kHz and (d) 5 – 50 kHz.

Table VI: Roughness Values of Bronze Surface.

Surface Finish	R_a microns (Average of 5 measurements)	Std. Dev. microns
250 grit SiC	0.51	0.04
400 grit SiC	0.10	0.02
600 grit SiC	0.12	0.02
6 micron diamond	0.06	0.02

Effect of Subsurface Corrosion or Gilding Delamination
A 0.0038mm thick Mylar interlayer was placed between the gilding and bronze substrate on 24K foil and leaf samples to serve as a simplified model for a nonconductive subsurface corrosion layer, or a delamination between between gilding layer and bronze substrate. Plots of the difference in resistance for samples with and without a Mylar interlayer are shown in Figure 10. Very little difference is seen in the foil gilded samples because the Mylar accounts for a much smaller percentage of the overall layer thickness. However, differences are seen for the leaf gilded samples, especially at the higher end of the frequency ranges.

The presence of the non-conducting Mylar between the gold layer and the bronze substrate affects the composite impedance, reducing the role of the bronze by effectively decreasing the penetration depth into the bronze. As given by the critical depth values, the changes in impedance due to the presence of Mylar interlayers are larger at the higher frequency portion of the probe's range. A similar response would be expected for samples with hidden corrosion underneath the gilding, although corrosion products are not totally non-conductive materials and the changes would not be expected to be quite as large as those seen for samples with Mylar interlayers. The size used on the leaf gilded samples also acts in the same manner, however its effect is small because of its extreme thinness.

Effect of Surface Corrosion, Coating Layer or Lift-off
To model the effect of a corrosion layer or coating above the gilding, Mylar of different thicknesses, given in Table VII, were placed between the probe and sample. These experiments also served as a model of the effect of lift-off on the measured probe impedance. The results of the measurements are graphed in Figure 11.

As the thickness of the non-conductive Mylar increases, the signal penetration into the sample decreases. For the bronze samples, the values represent lift off values and the change in impedance decreases with increasing Mylar thickness. As the Mylar gets thicker, the eddy currents are concentrated in an increasingly thin surface layer, causing the effect on the eddy currents of any microstructural or chemical features of the bronze surface layer, such as a worked surface or oxide layers, to be magnified. For samples where a composite measurement of the bronze and gilding layer is being measured, the contribution of the bronze is effectively decreased, resulting in an increase in the ?R. A change in sign of the impedance is seen where the composite impedance is greater than the impedance of the bronze substrate.

Table VII: Thickness of Mylar Placed Above Samples

Mylar type	Sheet thickness
Sample 16 from Table II.	0.0038 mm
Mylar A	0.028 mm
Mylar B	0.0505 mm
Mylar C	0.1375mm

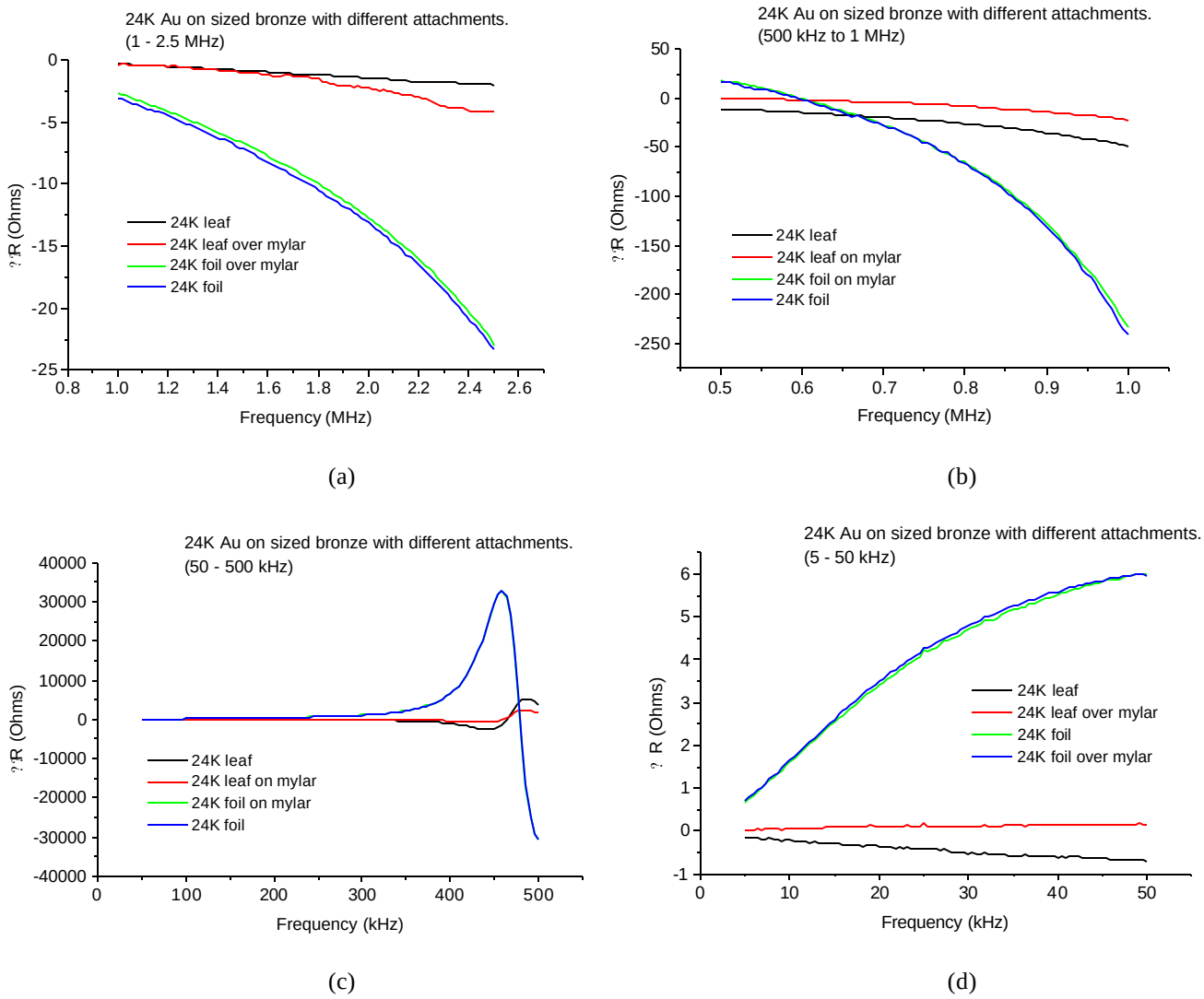
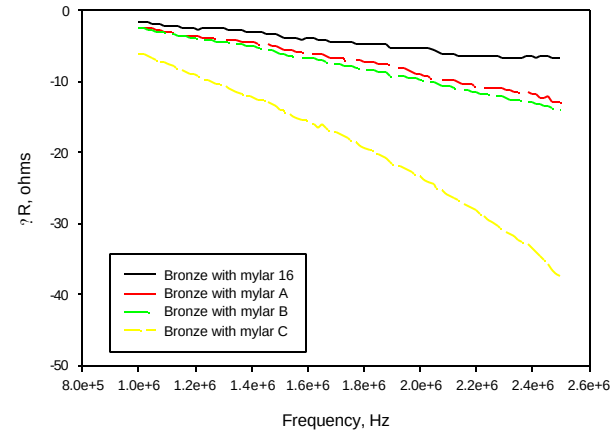
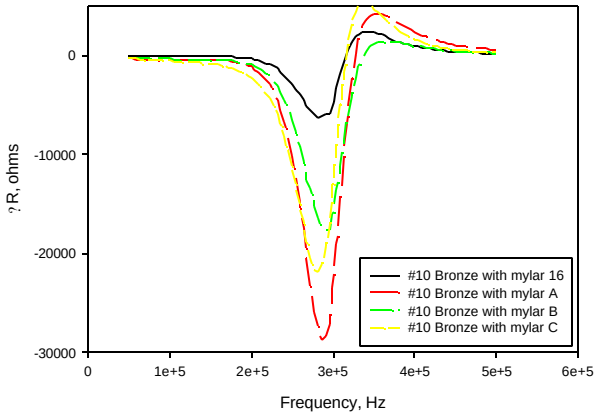


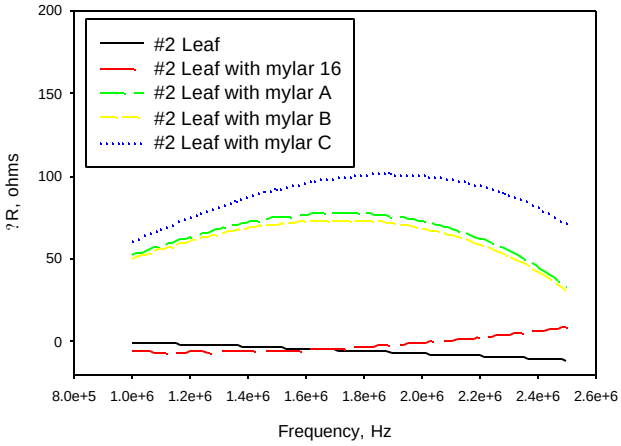
Figure 10: Frequency vs. ? R for 24K leaf and foil with and without a Mylar interlayer using (a) 1 – 2.5 MHz, (b) 500 kHz – 1 MHz, (c) 50 – 500 kHz) and (d) 5 – 50 kHz.



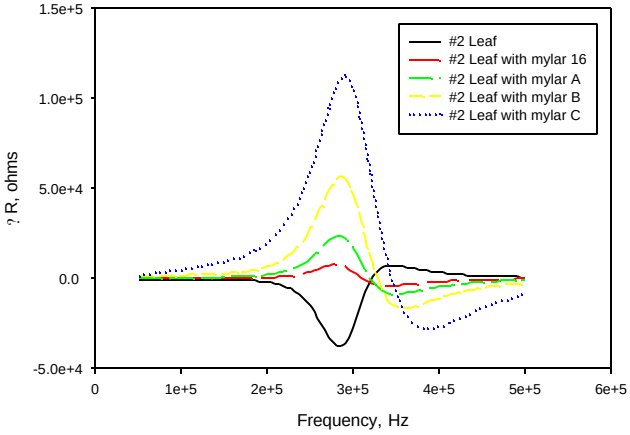
(a)



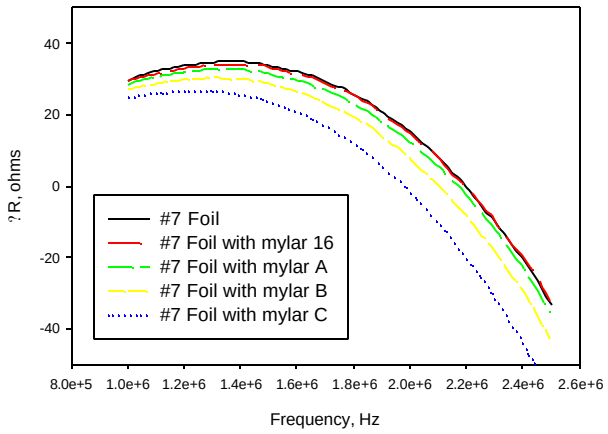
(b)



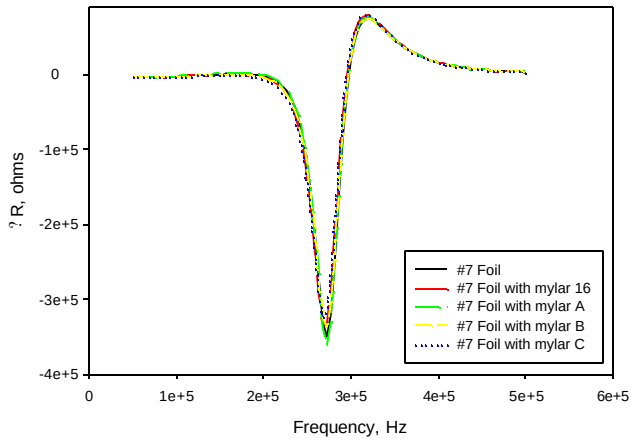
(c)



(d)



(e)



(f)

Figure 11. Frequency vs. ?R for samples with different thicknesses of Mylar between sample and probe. Ungilded bronze was examined using (a) 1 – 2.5 MHz and (b) 50 – 500 kHz. Leaf gilded bronze was examined using (c) 1 – 2.5 MHz and (d) 50 – 500 kHz. Foil gilded bronze was examined using (e) 1 – 2.5 MHz and (f) 50 – 500 kHz.

Results - Measurements on Freer Gallery of Art Bronzes

To test the effectiveness of the swept eddy current technique on actual gilded bronzes, several bronzes from the collection of the Freer Gallery of Art, including both previously studied bronzes of known gilding technology, and those whose gilding layers had not been previously analyzed, were examined in this study.

Several gilded bronzes, all previously determined to have been gilded using a mercury amalgam gilding technique, were selected for testing using the swept frequency eddy current method. Details about the bronzes are included in Appendix B. Measurements were made using spot probes for two frequency ranges, 1 - 2.5MHz and 50 - 500kHz. The results are shown in Figure 12. For the frequency range 1 - 2.5MHz, the change in probe impedance was positive for all objects. This is consistent with results for the mercury gilded reference samples. Results for the frequency range 50 - 500kHz are more difficult to interpret due to changes in signal polarity between the various samples, a trend also seen with the reference samples examined with this probe.

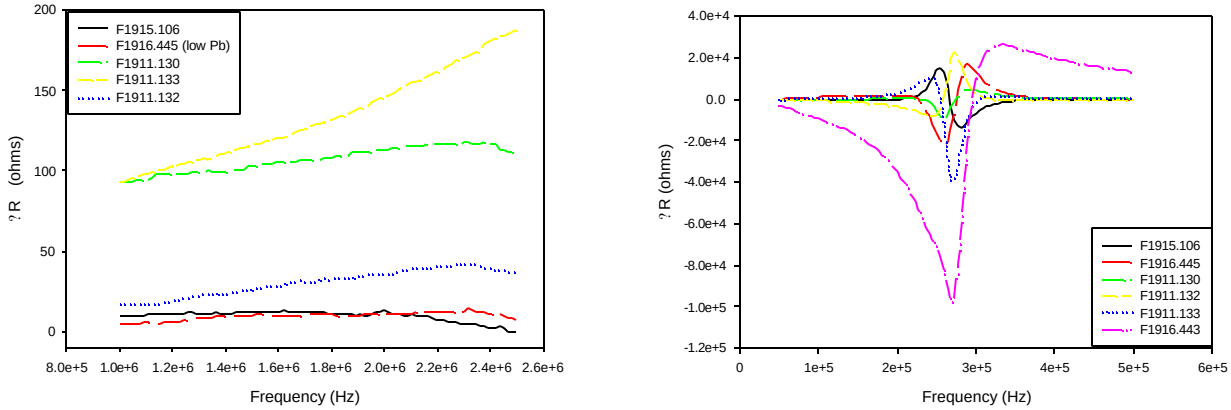
A large degree of variation was found in the mercury gilded measurements. It is likely that variation in the gilding layer is greater for an irregularly shaped surface than in the carefully prepared, flat reference samples described previously. This would be expected due to the nature of historic casting and metalworking technology. Several areas measured on a statuette: of Maitreya, accession number F1919.81, were found to have different probe impedances. However, the differences in impedance between different areas are larger than the variation between subsequent measurements made on the same area as seen in Figure 13. This indicates that signal averaging is an appropriate method to use for analyzing the data.

Measurements were made on a statuette of a water buffalo, accession number F1913.445, using two different bronze substrate areas for normalization measurements, one from an area with a green colored patina and the other from an area with a brown colored patina. The difference between the two results seen in Figure 14 indicates that a careful choice of bronze area for normalization is necessary. A measurement was made on the same bronze using a 50—500kHz pencil probe for comparison with the spot probe of the same frequency range. The results, plotted in Figure 14, are markedly different than those obtained with the spot probe.

A number of bronzes that had not previously been examined with metallography were also examined using eddy currents. The data for two bronze bear fittings of similar size and shape, accession numbers, F1917.514 and F1918.50, are plotted in Figure 15. Since the areas of remaining gilding on the rest of these bronzes were too small to facilitate measurement with the spot probes used for the majority of the experiments in this study, a pencil probe of frequency 50 - 500kHz was used. The results are plotted in Figure 16. Shifts are seen in the maxima and minima in measurements from some, but not all of the bronzes. Although greater variations are expected from the pencil probe, as it has a smaller active diameter than that of the spot probes used in the majority of the experiments, the degree of variation is also a measure of the uniformity of the surface. Due to variations in corrosion as well as in the gilding layer, for an effective measurement on corroded bronzes, the data from multiple areas must not be averaged together.

The results are not inconsistent with the results of the measurements on the mercury gilded reference sample. However, there is not enough information to state definitively that the bronzes are mercury gilded. Although the impedance of the one foil gilded object available for analysis, Figure 17, an E. Zhou dynasty plaque, accession number F1980.100, does exhibit opposite polarity to the other bronzes measured, its substrate is almost , if not completely, converted to corrosion products, precluding any true comparison to the reference samples studied. Measurements on gilded copper minerals may aid interpretation of results from such highly corroded gilded bronzes.

In general, the results from the 1—2.5 Mhz probe appear easier to interpret than those from the 50--500 kHz probe. The data suggest that the bronzes examined in this study are all probably mercury gilded, with the exception of F1980.100, which is known to be foil gilded. Therefore, further gilded bronzes need to be examined to prove the effectiveness of the technique on the range of gilding techniques found on bronzes. However, the results on the mercury gilded bronzes are similar to those seen for the mercury gilded reference sample, suggesting that a swept frequency eddy current technique should be effective.



(a) (b)

Figure 12: Frequency vs. ? R for mercury amalgam gilded bronzes using (a) 1 – 2.5 MHz and (b) 50 – 500 kHz.

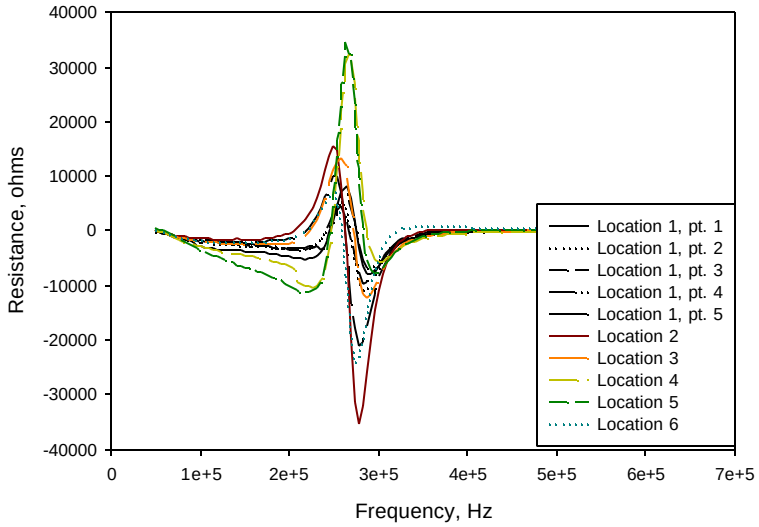
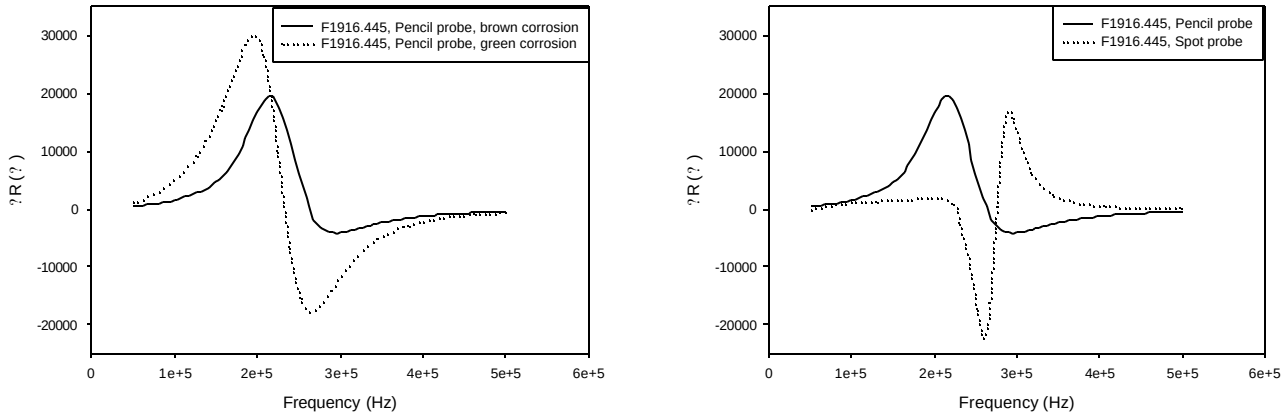
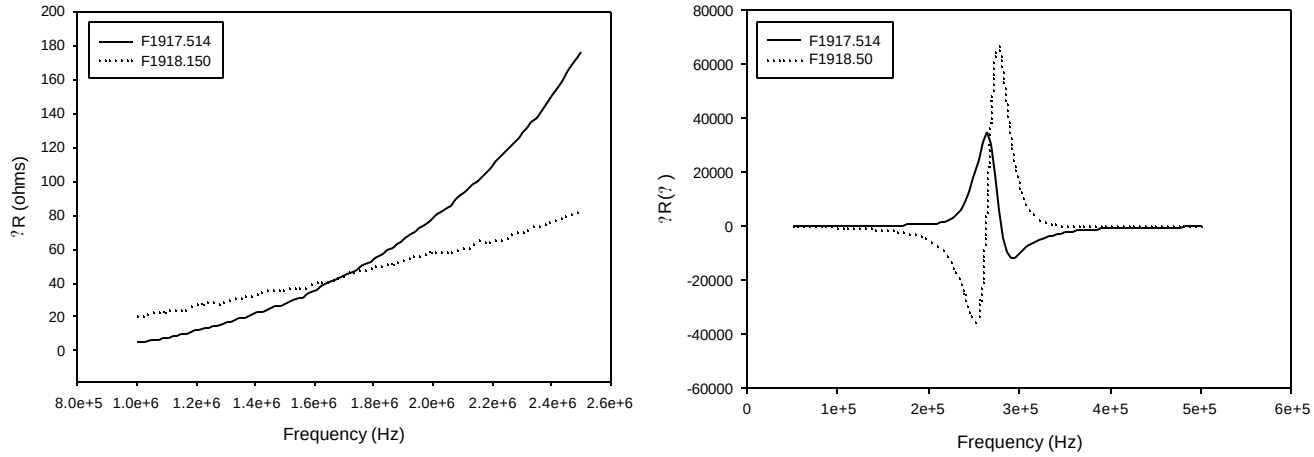


Figure 13: Frequency vs. ? R for six locations on F1919.81 using a 50 – 500 kHz spot probe. Duplicate measurements on one area are also plotted. All curves represent unaveraged measurements.



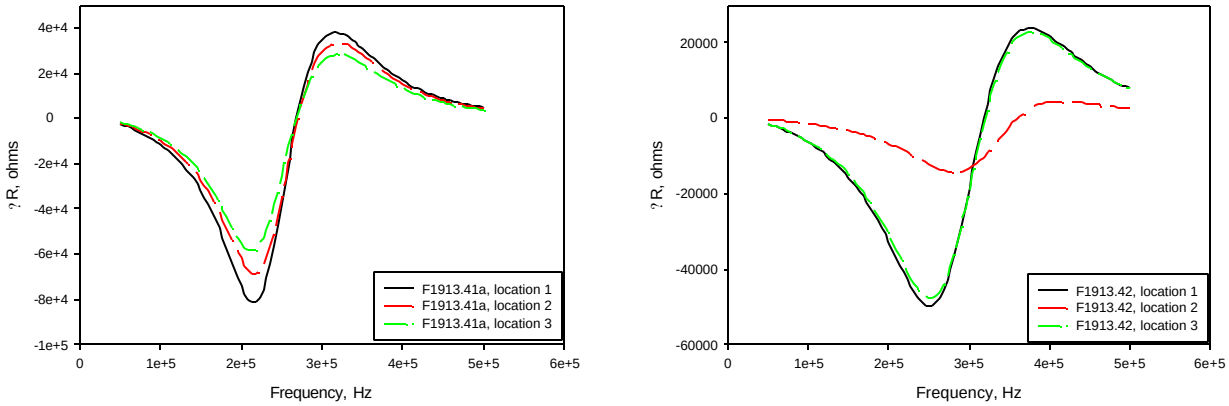
(a) (b)

Figure 14: Frequency vs. ?R for measurement of F1916.445 using 50 – 500 kHz. Data is plotted (a) using two different bronze substrate areas for normalization and (b) as results from both a spot probe and a pencil probe.



(a) (b)

Figure 15: Frequency vs. ?R for two samples of unknown gilding for (a) 1—2.5MHz and (b) a 50—500kHz spot probe. Measurements made in triplicate and averaged.



(a) (b)

Figure 16: Frequency vs. ?R for gilded samples using a 50 – 500 kHz pencil probe. Measurements made in triplicate and averaged at each of three locations for (a) F1913.41a and (b) F1913.42.

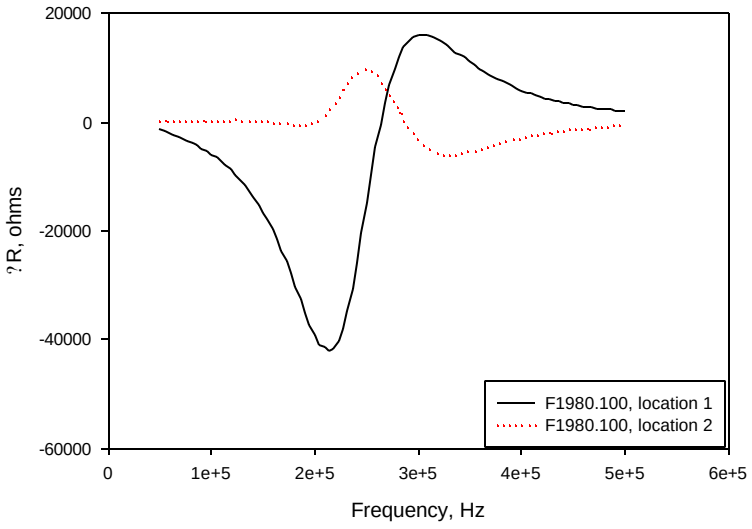


Figure 17. Frequency vs. ?R for F1980.100, a foil gilded plaque. Each curve is the average of three measurements.

Discussion

A number of material and physical parameters influence impedance measurements, including changes in composition, i.e. conductivity, changes in layer thickness, microstructure and surface roughness. These changes are manifested as a change in the response of the eddy current probes. There is a variation in the response of the probe to the different bronze compositions as seen in Figure 5, but also to differences in microstructure. Disk 16, similar in composition to sample 10, has a different impedance than that of sample 10. The disks were slow cooled and annealed, producing a large, even grained structure, while the ingot used to produce sample 10 was rapidly cooled resulting in a variable grain size. These differences in microstructure will produce a slightly different conductivity at the sample surface, resulting in differences in the impedance. The relative magnitude of the impedance for the different bronzes and pure metals was different for different frequency ranges, suggesting a frequency dependence in the measurements. This may be due to a number of parameters whose influence would vary with frequency, including, but not limited to, changes in phase angle, variations in surface microstructure and the presence of oxides on the surface of the metals. The variations in probe impedance caused by differences in composition and microstructure of the bronze substrate makes it necessary to compare changes in impedance, or a normalized impedance, rather than raw impedance measurements, when analyzing bronzes of unknown and varying compositions.

Roughness also plays a role, especially at the higher frequencies as seen in Figure 9a. A roughened surface may be modeled as a layer with areas of metal contact and areas of non-contact above the bulk metal. The impedance of the areas of metal contact is greater in magnitude than that of the areas of non-contact, which are analogous to areas with lift-off. As the degree of polish increases, the amount of lift-off in areas of non-contact decreases, causing an increase in probe impedance. This is similar to a decrease in lift-off, such as that seen in Figure 10a, as the thickness of the Mylar decreases. A decrease was seen in the ?R for the most highly polished sample. This may be attributed to the use of a different polishing media, diamond, and its effect on the bronze surface, possibly through formation of a different type of roughness profile or through surface hardening.

The behavior of the impedance may be modeled for three cases when analyzing materials with a surface layer with conductivity greater than the substrate material such as a gilded bronze. In the first case, the gilding layer thickness is less than the critical depth for gold and for bronze, $t_{\text{Au layer}} < t_{\text{cr(Au)}}$, $t_{\text{cr(bronze)}}$. This is the case for the 5 – 50 kHz and 50 – 500 kHz probe frequency ranges in which a true composite impedance will be measured. The changes in impedance resulting from changes in gilding layer thickness are fairly straightforward as shown in the data for the electroless plated and leaf gilded samples. Although gold has a higher resistance than pure copper, the resistance of all bronzes measured is greater than that of gold, hence the difference in the real impedance, ?R, of the gilded sample (a composite of the signal from the gold layer and the bronze) minus that of the bronze substrate is negative. As the thickness of the gilding layer increases, the lower resistance of gold becomes an increasingly large component of the composite impedance.

For the second case, the gilding layer thickness is greater than the critical depth of gold, but less than the critical depth of the bronze, $t_{\text{cr(Au)}} < t_{\text{Au layer}} < t_{\text{cr(bronze)}}$. As the thickness of the gold increases, there is no change in the contribution of the gold to the composite impedance, however, the gold at depths greater than the critical depth of gold acts to shield the bronze, in a similar manner as the Mylar interlayer used in some of the samples, reducing the amount of bronze in the region above the critical depth of bronze and effectively reducing its contribution to the composite impedance of the sample. As the contribution of the bronze continues to decrease, and the effective shielding continues to increase, ?R increases, becoming positive.

As the thickness of the gilding layer approaches the critical eddy current depth of bronze, the change in impedance, ?R, approaches the value of the impedance for gold of the same composition minus the impedance of the bronze substrate, shown in Figure 18 where the real impedance for 24K gold minus the real impedance for bronze has been plotted as a function of frequency. There is no further change in the impedance resulting from thickness changes as gilding layer thickness increases beyond this point. ?R is no longer a composite impedance but is that for the gold layer alone, defining the third case, $t_{cr(Au)}$, $t_{cr(bronze)} < t_{Au\ layer}$. This is the case for the foil gilded sample in the frequency ranges 1 - 2.5 MHz and 500kHz - 1MHz. The various thicknesses which divide these cases are dependant on the probe frequency being used and the frequency range being measured.

For most measurements, the higher frequency range of the probe was best able to discriminate between the different gold leafs. This is supported by the calculation for t_{cr} for bronze and gold shown in Figure 2. The critical depth for gold is only 2.25 ?m at 2.5 MHz so that changes in gold leaf thickness will be magnified at higher frequencies. Since the critical depth for bronze is much higher, the probe impedance will necessarily be affected by changes in the composite impedance rather than by the changes in the gold layer thickness alone.

The mercury gilded layer was expected to appear similar to the foil gilded layer since for both, the thickness is near or greater than the gold critical depth for the majority of the frequencies measured. However, the resistivity of gold has been shown to increase with the addition of mercury (Gmelin 1954). This increase should continue until the formation of an intermetallic compound at approximately 20% mercury. In studies of mercury gilded Chinese bronzes (Jett 1993), mercury contents were found to vary from zero to 20% with the highest values located in a less than one micron thick layer at the center, in depth, of the gilding layer. The microstructure of

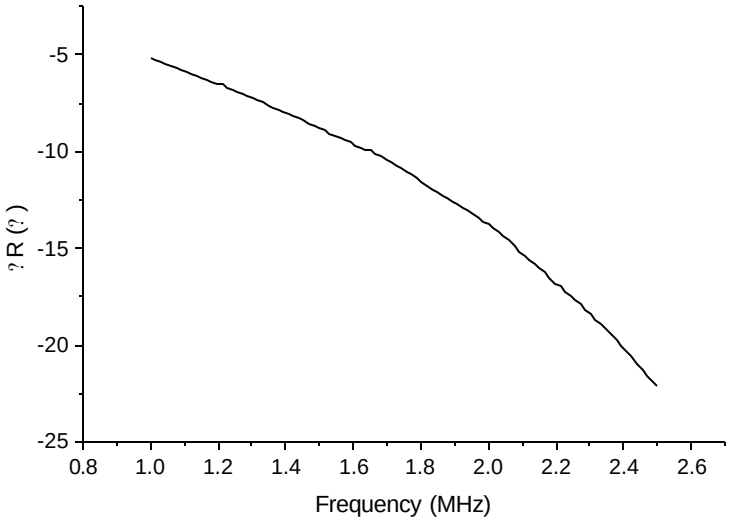


Figure 18: Frequency vs. ?R for gold, reference sample 15, minus bronze, reference sample 10 for 1-2.5MHz.

a mercury gilding layer is also very different than the other types of gilding examined in this study. It has a large amount of included porosity, compacted, especially near the surface, from burnishing. Researchers have found that the change in the impedance increased with increasing diameter of a void in aluminum(Satveli et al. 1996). As they were only examining a single void, the relative effects of size and amount of porosity are unclear. In addition, as the impedance of air is much higher than either bronze or gold, the composite impedance of this gilding layer, the impedance of a gold-mercury alloy and air, is greater than that of bronze, resulting in a positive value of the change in impedance after the subtraction of the impedance of the bronze substrate. The effect is greatest for the higher frequency probes where the thickness of the mercury amalgam gilded layer is greater than the critical depth for the eddy currents. Thus the impedance of the gilding layer dominates the composite impedance measured.

Note should be made that the error in measurement is greatest at the upper end of the probe frequency range, shown in Figure 19. More error was expected in the samples of mercury amalgam gilded bronzes than in those of the leaf gilded bronzes, due to inherent variations in gilding thickness found in the mercury gilded layers. This was not found to be the case for these reference samples. Further errors in the experimental results include those due to probe heating during the measurement period.

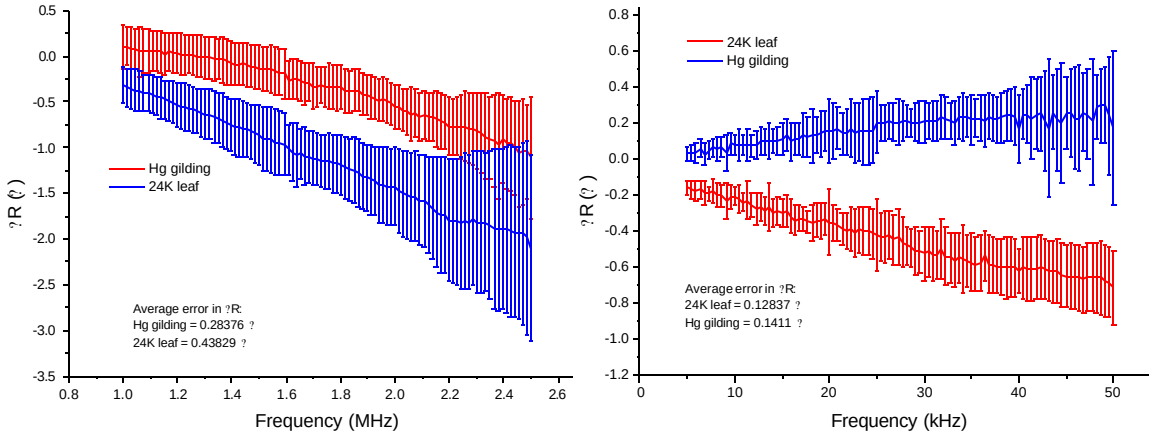


Figure 19: Frequency vs. ?R with error bars for Hg gilded bronze and 24K leaf gilded bronze for (a) 1 – 2.5 MHz and (b) 5 – 50 kHz.

Conclusions

Results have been presented which show that eddy current testing can be used to discriminate between gilding techniques on a bronze substrate. Better discrimination between different compositions of leaf gilded samples is obtained at higher frequencies.

The results of this study suggest that using two swept frequency measurements, one at high frequency and one at low frequency, it may be possible to use the following criteria to assign gilding method to a sample from the analysis of plots of ?R vs. frequency:

1) Leaf gilding: Small, negative slope for both low and high frequencies. Areas of single leaf and double (overlapping) leaf switch relative magnitudes from low to high frequency.

2) Electrochemical gilding: Very small negative value very near zero at both low and high frequencies.

3) Mercury gilding: Small negative value, negative slope at high frequency, with a change in polarity to positive values, positive slope at low frequencies.

4) Foil gilding: Large negative values at high frequency, with a change in polarity to large positive values at high frequency.

Note that as the impedance characteristics of each probe are different, it is not possible to predict values for ?R. Rather, it is necessary to characterize the specific probe, prior to making measurements on unknowns. Commercial probes were used in this study so that the method could be more easily duplicated. It is likely, however, that differences between commercial probes of the same model will also exhibit variations in their impedance characteristics. To characterize the probe, a series of reference measurements will be necessary prior to using a new probe to measure gilding layer properties.

Results can be affected by a number of physical factors including surface roughness and probe lift-off. Higher frequency measurements are also affected by changes in surface roughness. Differences in the bronze composition and microstructure will affect the composite impedance, although this is minimized at the highest frequencies. This makes it unlikely that the method can be used for direct quantitative measurements of thickness and conductivity of the gilding layers on bronzes of unknown composition and microstructure.

Model experiments for subsurface corrosion or delamination showed impedance changes occur, especially for thin gilding layers. Model experiments show that a decrease in impedance at high frequencies and an increase at low frequencies can be expected for coated samples, samples with corrosion at the surface or in cases of lift-off. However, variations in probe liftoff can be avoided by placing the probe directly on the sample. A piece of Mylar can be placed between the probe and sample surface in order to protect the object. Several samples were examined using a protective piece of 3 mil Mylar which shifted the curves by a constant value. The value could be easily corrected for if all measurements were made with the same thickness of Mylar.

For the measurements made on real bronzes, mercury gilded bronzes from the Freer collection had positive changes in impedance for the frequency range 1 - 2.5MHz. This is consistent with results found for the reference samples. Results from the 50 - 500kHz probe were not as clear, although the foil gilded bronze studied was distinguishable from the mercury gilded bronzes by a difference in polarity.

Acknowledgements

The authors acknowledge Dr. Robert E. Green Jr. of the Center for Nondestructive Evaluation, The Johns Hopkins University for the use of the impedance analyzer and laboratory space, Paul Jett from the Freer Gallery of Art for mercury gilding a sample for analysis and to the National Center for Preservation, Technology and Training, who graciously provided the funding for the study.

References

ASNT. 1986. *Electromagnetic Testing*. Edited by R. C. McMaster, P. McIntire and M. L. Mester. Vol. 4, *Nondestructive Testing Handbook*.

ASTM. 1998. Annual Book of ASTM Standards. In *Standards B244, B487, B504, B567,B568, B588.*

Bartolini, M., B. Colombo, M. Marabelli, A. Marano, and C. Parisi. 1997. Non-destructive Tests for the Control of Ancient Metallic Artifacts. Paper read at Metal 95.

Bowler, John. 2001. Personal Communication.

Brainin, E. I., G. S. Kokarev, V. A. Kolotii, A. I. Polyakova, and B. K. Tsymbarenko. 1993. Eddy-Current Inspection of the Thickness of Zinc Coating on Parts made of casting aluminum alloy. *Russian Journal of Nondestructive Testing* 28 (3):230-233.

Bray, W. 1993. Techniques of gilding and surface enrichment in pre-Hispanic American metallurgy. In *Metal Plating and Patination*, edited by S. L. Niece and P. Craddock. Oxford: Butterworth Heinemann.

Cunningham, Tony. 1995. Measuring Dry Film Thickness Using Electromagnetic and Eddy Current gauges. *Coatings and Linings* (May):39-41.

de Halleux, B., A. Ptchelintsev, and B. de Limburg Stirum. 1997. Thickness and conductivity determination of thin coatings on ferromagnetic substrates in the case of cylindrical symmetry. *Rev. Sci. Instruments* 68 (9):3533-3537.

Dodd, C. V., and W. E. Deeds. 1968. Analytical Solutions to Eddy-Current Probe-Coil Problems. *Journal of Applied Physics* 39 (6):2829-2838.

Drayman-Weisser, Terry. 2000. *Gilded Metals, History, Technology and Conservation*: Archetype Publications Ltd.

Gmelin Institute. 1954. *Gold*. 8 ed. Vol. 62, *Gmelins Handbuch der Anorganischen Chemie*. Weinheim/Bergstrasse: Verlag Chemie, GMBH.

Hagemaier, D. J. 1990. *Fundamentals of Eddy Current Testing*: ASNT.

Harrison, D. H., L. D. Jones, and S. K. Burke. 1996. *Journal of Nondestructive Evaluation* 15 (21).

Jett, Paul. 1993. A Study of the Gilding of Chinese Buddhist Bronzes. In *Metal Plating and Patination*, edited by S. L. Niece and P. Craddock. Oxford: Butterworth Heinemann.

Lechtman, H. 1973. The gilding of metals in Pre-Columbian Peru. In *Application of Science in Examination of Works of Art*, edited by W. J. Young. Boston: Boston Museum of Fine Arts.

Lechtman, H. 1979. A pre-Columbian technique for electrochemical replacement plating of gold and silver on copper objects. *Journal of Metals* 31 (12):154-160.

Mach, M., G. Poehlmann, and V. Stoeckle. 1991. Die Messung von Patinaschichtdicken auf Kupfer und Bronze mit Hilfe Des Wirbelstromverfahrens. *Wiener Berichte ueber Naturwissenschaft in der Kunst* 6/7/8:211-215.

Marabelli, Maurizio, and Marcello Medori. 1991. Il metodo delle "eddy currents" per l'esame strutturale dei monumenti in bronzo. *Materiali e Strutture* 1 (3):111-120.

Mel'nikov, I. V., E. N. Semenov, R. K. Trushkevich, and K. S. Doronin. 1998. Eddy Current Inspection of the Properties of Surface Layers of Components after in-feed grinding. *Russian Journal of Nondestructive Testing* 34 (5):345-350.

Moulder, John C., Mark W. Kubovich, Erol Uzal, and James H. Rose. 1995. Pulsed eddy-current measurements of corrosion-induced metal loss: theory and experiment. *Rieview of Progress in Quantitative Nondestructive Evaluation* 14:2065-2072.

Moulder, John C., Sunil K. Shaligram, Jay A. Bieber, and James H. Rose. 2000. Pulsed eddy current inspections and the calibration and display of inspection results. U.S.: Iowa State University Research Foundation, Inc.

Moulder, John C., Erol Uzal, and James H. Rose. 1992. Thickness and conductivity of metallic layers from eddy current measurements. *Rev. Sci. Instrum.* 63 (6):3455-3465.

Mundry, E., and J. Riederer. 1988. Kunst- und Kulturwissenschaftliche Untersuchungen mit Zerstoerungsfreien Methoden. *Praktische Metallographie* Sonderband:9-28.

Norton, Stephen J., Arnold H. Kahn, and Michael L. Mester. 1989. Reconstructing Electrical Conductivity Profiles from Variable-Frequency Eddy Current Measurements. *Research in Nondestructive Evaluation* 1:167-179.

Oddy, W. A. 1993. Gilding of metals in the Old World. In *Metal Plating and Patination*, edited by S. L. Niece and P. Craddock. Oxford: Butterworth Heinemann.

Palmer, B. S., H. D. Drew, and R.S. Decca. 2000. Scanning eddy current dynamometer with 100micrometer resolution. *Review of Scientific Instruments* 71 (8):3168-3172.

Sandovskii, V. A. 1994. Optimization of Eddy Current Inspection of Coatings. *Russian Journal of Nondestructive Testing* 30 (4):265-270.

Satveli, Radhika, John C. Moulder, Bing Wang, and James H. Rose. 1996. Impedance of a coil near an imperfectly layered metal structure: The layer approximation. *Journal of Applied Physics* 79 (6):2811-2821.

Scott, D. A. 1983. Depletion gilding and surface treatment of gold alloys from the Narino area of ancient Colombia. *Journal of the Historical Metallurgy Society* 17 (2):99-115.

Sethuraman, Ananth, and James H. Rose. 1995. Rapid Inversion of Eddy Current Data for Conductivity and Thickness of Metal Coatings. *Journal of Nondestructive Evaluation* 14 (1):39-46.

Silkin, V. Ya., and A. E. Ponomarev. 1994. Measurement of Coating Thickness by the Eddy Current Method. *tr. from Izmeritel'naya Tekhnika* 9:27-28.

Tai, Cheng-Chi. 2000. Characterization of coatings on magnetic metal using the swept-frequency eddy current method. *Review of Scientific Instruments* 71 (8):3161-3167.

Tai, Cheng-Chi, James H. Rose, and John C. Moulder. 1996. Thickness and conductivity of metallic layers from pulsed eddy-current measurements. *Review of Scientific Instruments* 67 (11):3965-3968.

Uzal, Erol, John C. Moulder, Sreeparna Mitra, and James H. Rose. 1993. Impedance of coils over layered metals with continuously variable conductivity and permeability: Theory and experiment. *J. Appl. Phys.* 74 (3):2076-2089.

Appendix A: Analyses of Bronze Disks

Wet chemical analyses performed by Mrs. I.V. Bene in 1963/64. Values given are the average of duplicate analyses. The bronze disks were cast and slow cooled.

Bronze disks	Cu	Sn	Pb	Total
1	97.9	0.5	0.5	98.9
2	0.04	98.3	0.6	98.9
3	---	0.04	98.9	98.9
4	94.5	3.1	0.4	98.0
5	89.8	8.8	0.4	99.0
6	88.2	10.2	0.6	99.0
7	85.8	12.3	Tr	98.1
8	83.9	14.6	0.5	99.0
9	94.4	1.6	1.9	97.9
10	90.3	6	1.9	98.2
11	84.7	11.8	1.8	98.3
12	90.4	5.2	1.9	97.5
13	87.9	5.5	4.4	97.8
14	83.6	4.4	9.2	97.2
15	76.1	13.1	9.2	98.4
16	80.5	8	9.7	98.2

Appendix B: Freer Gallery of Art Bronzes examined using Eddy Currents

Accession Number	Object	Object provenance	Gilding method	Comments
F1915.106	Sarcophagus	Tang. 8c. A.D.	Hg gilding	Metallography done
F1911.130	Statuette of Buddhas Duobao and Sakyamuni	6 Dyn., (220-589 A.D.)	Hg gilding	Metallography done
F1911.132	Statuette: Guanyin	6 Dyn., 518 A.D.	Hg gilding	Metallography done
F1911.133	Statuette: Buddha	6 Dyn., (220-589 A.D.)	Hg gilding	Metallography done
F1919.81	Statuette: Maitreya	N. Chi, 561 A.D.	Hg gilding	Metallography done
F1916.443	Garment clasp	E. Zhou-W. Han, (770 B.C.-9 A.D.)	Hg gilding	Metallography done
F1916.445	Statuette: water buffalo	Song (960-1279A.D.)	--	Low lead content
F1916.394	Statuette: Lion	Song (960-1279A.D.)	--	Brass
F1917.514	Fitting: Bear	Han (206-220A.D.)?	--	----
F1918.50	Fitting: Bear	Han (206-220A.D.)?	--	----
F1913.41a	Statuette	Sui (581-618 A.D.)?	--	pure Cu and Sn
F1913.42	Statuette: Guanyin	Sui (581-618 A.D.)	--	low lead
F1980.100	Plaque	E. Zhou (770-221 B.C.)	Foil gilded	little if any bronze remains

Appendix C: Time Domain Measurements

Eddy currents result from the interaction of time varying magnetic fields with a conductive sample. The work described in the body of this report assesses the effect of variations in the conductivity and thickness of gilding layers on the impedance of a probe coil in a range of frequencies. In the work described briefly in this appendix, undertaken at the end of the grant period, a different measurement approach was followed. The change in electrical potential across the probe was monitored as a function of time following the application of a pulsed driving current.

Studies undertaken at Iowa State University have examined the use of pulsed eddy current measurements to study the presence of layer thinning due to corrosion in aluminum and the measurement of thickness and conductivity of conducting surface layers on metallic substrates. In one study, Moulder et. al. used a 5V TTL square wave excitation source, and recorded the resulting current as a function of time during the first half of the pulse(Moulder et al. 1995). They found that the maximum in signal amplitude and the time at which the signal became negative varied depending on the amount of metal lost. The presence of non-conductive spacers placed between the surface layer and substrate resulted in signals comparable to those for metal loss, however the time scale of the response was shorter. They felt this might be exploited to determine the presence of corrosion verses the loss of contact in a metal to metal bond. They were able to model their results by calculating the admittance (the inverse of the impedance) and then applying Fourier transform techniques to obtain the time domain current profile. They have patented a pulsed eddy current instrument and analysis system (Moulder et al. 2000) and are currently designing a portable version (Bowler 2001). The patent does not mention measurement of conductive surface layers.

Tai et. al. used pulsed eddy currents to measure a series of samples with conducting layers of varying thickness(Tai, Rose, and Moulder 1996). They used three features of the measured current signal curve to determine thickness and conductivity of the surface layers: the maximum or minimum in signal amplitude, the arrival time of the maximum/minimum, and the zero crossing time. The changes in signal amplitude are nearly linear with changes in conductivity differences between the substrate and the surface layer. The signal amplitude was found to vary most strongly of the three parameters with changes in surface layer thickness until the thickness of the surface layer exceeded the skin depth. At that point, the amplitude becomes insensitive to layer thickness. Significant error was found to be introduced by thermal effects such as coil heating, affecting the position of the zero crossing time in particular. Thus, the zero crossing time was given a lower weight in the data analysis. Independent determinations of thickness and conductivity were made down to approximately 50 microns. With thinner surface layers only thickness or conductivity could be independently determined, not both. Advantages of the pulsed eddy current method over the swept frequency method include the speed of measurement, which makes probe wobble less of a factor in reproducible measurements, and the lower cost of instrumentation.

For the measurements described below, the coil probes were excited with a 5V TTL square wave, cycled at 1kHz that was generated by an HP3325B synthesizor/function generator. Measurements were made on samples No. 2, 5, 7 and 10 using a Lecroy 9450A digital oscilloscope during the first half of the square wave. The response to 500 pulses was averaged. All measurements were normalized by a reference measurement from an ungilded bronze sample. The voltage measured for the ungilded bronze was subtracted from the voltage measured for the gilded samples. The results for the gilded samples, No's. 2, 5, and 7 are shown in Figure A2.1a-d.
All four probes were able to discriminate between the leaf and foil gilded samples. The higher frequency probe (1-2.5MHz) could additionally discriminate between the two leaf samples. Differences in signal shape for different samples suggests that further information may be obtained

from applying Fourier analysis techniques to the time domain signals. These differences are particularly noticeable in Figures A2.1a-b.

This initial investigation indicates that the method shows promise for characterizing gilding layers and determining gilding technique. Further experimentation with a wider range of samples is planned. If successful, this could result in a more rapid and less expensive method of analysis than swept eddy current measurements.

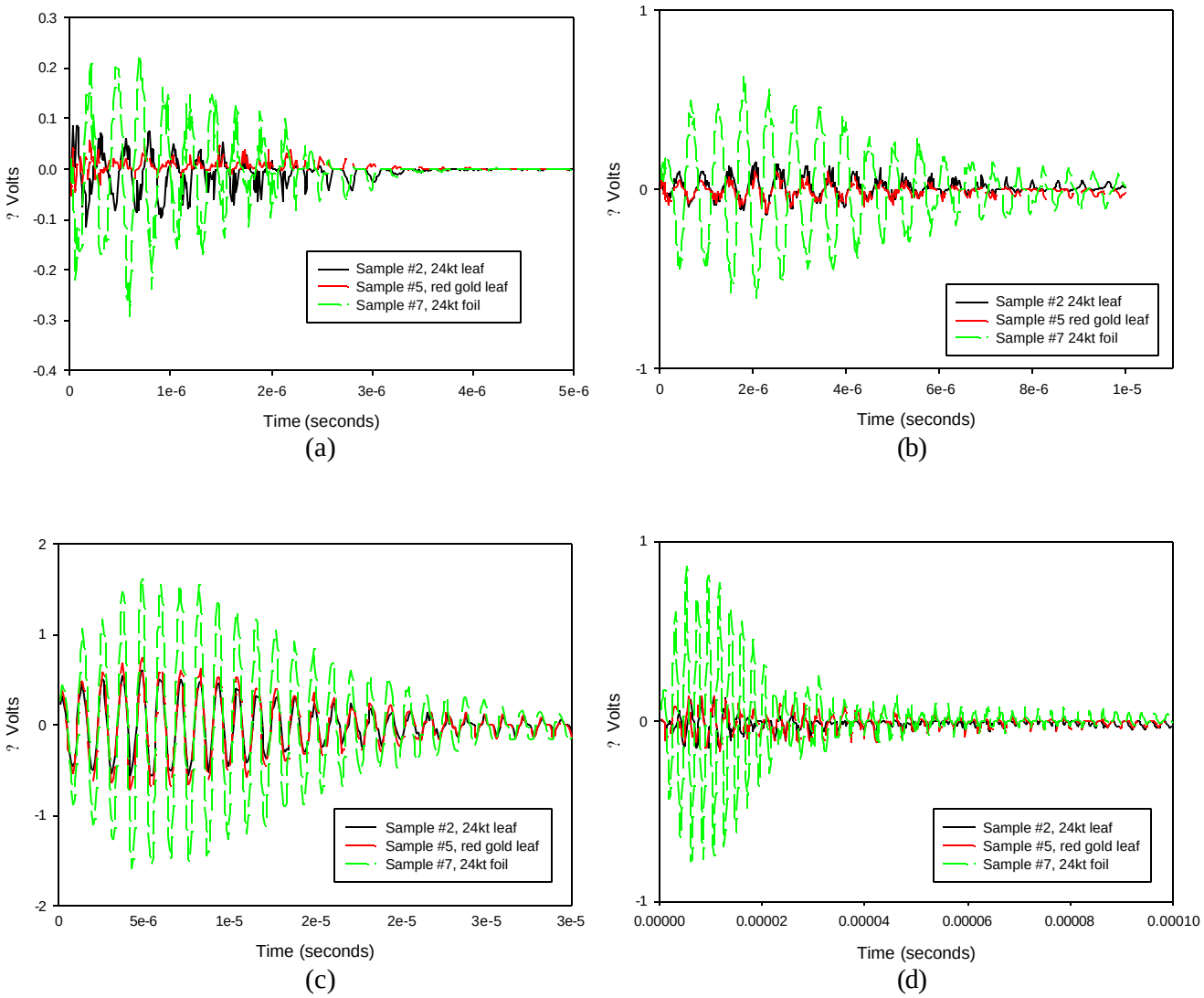


Figure A2.1a-d. Change of voltage with time for gilded samples measure with four different probes.